

Why earthquakes correlate weakly with the solid Earth tides: Effects of periodic stress on the rate and probability of earthquake occurrence

N. M. Beeler and D. A. Lockner

U.S. Geological Survey, Menlo Park, California, USA

Received 20 September 2001; revised 14 February 2003; accepted 3 April 2003; published 22 August 2003.

[1] We provide an explanation why earthquake occurrence does not correlate well with the daily solid Earth tides. The explanation is derived from analysis of laboratory experiments in which faults are loaded to quasiperiodic failure by the combined action of a constant stressing rate, intended to simulate tectonic loading, and a small sinusoidal stress, analogous to the Earth tides. Event populations whose failure times correlate with the oscillating stress show two modes of response; the response mode depends on the stressing frequency. Correlation that is consistent with stress threshold failure models, e.g., Coulomb failure, results when the period of stress oscillation exceeds a characteristic time t_n ; the degree of correlation between failure time and the phase of the driving stress depends on the amplitude and frequency of the stress oscillation and on the stressing rate. When the period of the oscillating stress is less than t_n , the correlation is not consistent with threshold failure models, and much higher stress amplitudes are required to induce detectable correlation with the oscillating stress. The physical interpretation of t_n is the duration of failure nucleation. Behavior at the higher frequencies is consistent with a second-order dependence of the fault strength on sliding rate which determines the duration of nucleation and damps the response to stress change at frequencies greater than $1/t_n$. Simple extrapolation of these results to the Earth suggests a very weak correlation of earthquakes with the daily Earth tides, one that would require >13,000 earthquakes to detect. On the basis of our experiments and analysis, the absence of definitive daily triggering of earthquakes by the Earth tides requires that for earthquakes, t_n exceeds the daily tidal period. The experiments suggest that the minimum typical duration of earthquake nucleation on the San Andreas fault system is ~ 1 year. *INDEX TERMS*: 1249 Geodesy and Gravity: Tides—Earth; 7209 Seismology: Earthquake dynamics and mechanics; 7215 Seismology: Earthquake parameters; 8010 Structural Geology: Fractures and faults; 8159 Tectonophysics: Rheology—crust and lithosphere; *KEYWORDS*: earthquake probability, stress triggering, earthquake nucleation

Citation: Beeler, N. M., and D. A. Lockner, Why earthquakes correlate weakly with the solid Earth tides: Effects of periodic stress on the rate and probability of earthquake occurrence, *J. Geophys. Res.*, 108(B8), 2391, doi:10.1029/2001JB001518, 2003.

1. Introduction

[2] If increases in static stress trigger earthquakes [e.g., Stein, 1999], why do the solid Earth tides not trigger earthquakes [Cotton, 1922; Klein, 1976; Heaton, 1982]? Tidal forces exerted by the Moon and Sun produce continuously varying stresses in the Earth's crust with daily maximum shear stressing rates that are 2 orders of magnitude larger than the rate of accumulation of stress along active faults due to plate motion [Heaton, 1982]. If faults failed at a threshold level of stress, e.g., a Coulomb failure criterion as assumed in studies of static stress triggering, earthquake rates would correlate directly with the stressing rate and therefore with Earth tides [e.g., Heaton, 1982;

Lockner and Beeler, 1999]. In contrast, careful analyses of quality data sets suggest little or no correlation between Earth tides and earthquakes [e.g., Vidale *et al.*, 1998]. Apparently a threshold failure criterion does not completely characterize earthquake failure. This conclusion is suggested by other seismological observations; for example, in studies of static stress change, stress increases of less than 0.01 MPa show no correlation with increased seismicity [e.g., Reasenber and Simpson, 1992; Simpson and Reasenber, 1994; Hardebeck *et al.*, 1998].

[3] As for natural faults, the laboratory fault failure criterion is not a threshold [Johnson, 1981]. The primary characteristics of failure on laboratory-scale faults are shown in Figure 1a:

[4] 1. For faults loaded at a constant rate V_L , measurable fault slip δ accrues prior to failure. Such slip leads to a deviation from a linear (elastic) increase in shear stress τ

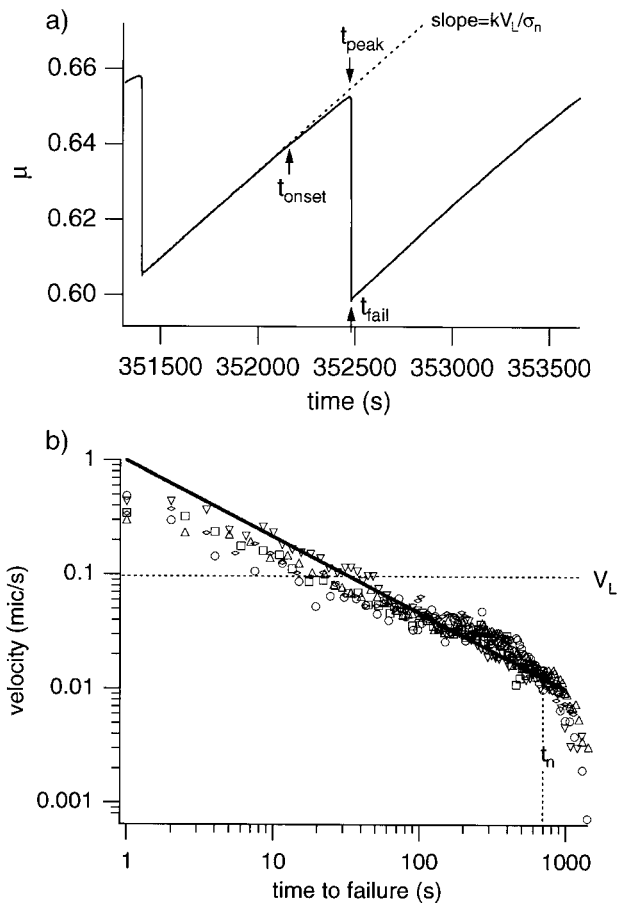


Figure 1. Stick-slip. (a) Frictional stress, μ , the ratio of shear stress τ to normal stress σ_n , versus time during sliding between initially bare surfaces of Westerly granite at room temperature, 50 MPa confining pressure, and $0.1 \mu\text{m s}^{-1}$ loading velocity. The onset of detectable slip (t_{onset}) occurs when stress deviates from the dashed elastic loading curve. The onset of detectable slip and the peak stress (t_{peak}) differ from the failure time (t_{fail}). The delay between the onset of detectable slip and the eventual failure time is ~ 180 s. (b) Acceleration to failure during slip of a fault in granite at room temperature and 50 MPa confining pressure. Data from five successive failure events in the test shown in Figure 1a [after Dieterich and Kilgore, 1996]. The reference line has a slope of -1 . Sliding velocity increases as failure is approached. The duration of nucleation is ~ 700 s. The peak stress is reached when the sliding velocity reaches V_L (horizontal dashed line). At all times prior to peak strength, the sliding velocity is increasing while the fault strength is increasing (Figure 1a), indicating that strength has positive rate dependence.

with time t ; shear stress on the fault is $\tau = k(V_L t - \delta)$, where k is the combined stiffness of the experimental apparatus and the sample.

[5] 2. Peak stress occurs prior to failure indicating no instantaneous threshold failure stress.

[6] 3. Failure is delayed; there is lag time between the onset of detectable slip (t_{onset}), or the time of peak stress (t_{peak}), and the time of failure (t_{fail}), defining a measure of

the duration of nucleation, e.g., $t_n = t_{\text{fail}} - t_{\text{onset}}$. In experiments conducted by Lockner and Beeler [1999] loaded at $V_L = 0.1 \mu\text{m s}^{-1}$, t_n measured in this approximate way is 100–800 s, and during nucleation the sliding velocity increases monotonically until failure is reached (Figure 1b) [Dieterich, 1992]. As we will argue later in this paper, understanding the origin of this delay is key to understanding why earthquake occurrence correlates weakly with small stress changes such as the solid Earth tides. Delayed failure is also manifest in another long-known and related phenomenon known in mechanical engineering, material science, and rock mechanics as “static fatigue,” an inherent time delay between the application of a stress increase and the occurrence of rock failure, or the occurrence of an unstable stress drop, induced by the stress change [e.g., Griggs, 1936; Scholz, 1972; Kranz, 1980].

[7] That the largely uncorrelated response of natural seismicity to tidal stress might be an additional consequence of time-dependent or delayed failure has been noted previously. On the basis of early experiments on static fatigue Knopoff [1964, p. 1869] suggested that stress increases equivalent to the tidal stress amplitude would induce failure following a delay of months or even years. He concluded that earthquakes would not correlate with periodic stressing of such small amplitude. Similarly, Rydelek *et al.* [1992, p. 133] concluded that the lack of correlation between earthquake occurrence and the tides indicates that failure is intrinsically time-dependent with a characteristic time greater than the tidal period. To establish a direct connection between delayed failure and the absence of tidal triggering, Lockner and Beeler [1999] undertook a systematic study of the sensitivity of failure time to periodic stressing. Earthquake catalogues were generated using laboratory-scale faults undergoing quasiperiodic failure, “stick-slip”, which is the laboratory equivalent of the earthquake cycle [Brace and Byerlee, 1966]. Faults were stressed to failure by the combined action of a constant loading rate and a small-amplitude periodic stress. Lockner and Beeler [1999] observed a strong correlation between the periodic stress and the occurrence of failure at shear stress amplitudes above approximately 0.3 MPa. As the periodic forcing amplitude decreased, the correlation of failure with the periodic stress also decreased to the degree that below amplitudes of 0.1 MPa, confidence that events were correlated was reduced to less than 60% for catalogs of approximately 20 events. Their qualitative interpretation of these observations is that the process(es) responsible for the characteristic delay of failure damps the response of faults to small amplitude stress perturbations. They concluded that the small amplitude of the tidal stress in the Earth generates weakly correlated seismicity and predicted that approximately 1% of earthquakes should correlate with the daily tides.

[8] In the present study we further analyze and model the previous experimental results of Lockner and Beeler [1999]. Our analysis reveals two modes of response of laboratory fault populations to periodic stress: a correlated response consistent with simple threshold models such as Coulomb failure, and a different response where expected correlation is significantly suppressed. The former response is observed when the periodic component of the forcing stress exceeds a critical duration. We note that the critical duration or critical time is expected based on previous rock deformation experi-

ments and that it corresponds with the duration of nucleation (Figure 1). To extrapolate our particular laboratory observations, we develop formal expressions for the probability that a population of N earthquake failure times are correlated with a periodic stress for both observed response modes. By assuming that natural earthquake failure is similar to our experiments, we predict the number of events required to detect a correlation between earthquakes and the tides and compare the predictions with seismological observations. By extrapolating the laboratory observations we also estimate the critical time expected under natural rates of tectonic stressing.

2. Experiments

[9] The experiments of *Lockner and Beeler* [1999] were conducted on saw cut fault surfaces of Westerly granite inclined 30° to the cylindrical sample axis (Figure 2). Samples were deformed in a triaxial loading frame at constant confining pressure of $\sigma_2 = \sigma_3 = 50$ MPa, where the greatest, intermediate, and least principal stresses are σ_1 , σ_2 , and σ_3 , respectively. The constant axial shortening rates imposed are equivalent to sliding rates of $V_L = 0.001$, 0.01 , or $0.1 \mu\text{m s}^{-1}$ resolved onto the fault surface. The constant loading rate was modulated by a sine wave with a frequency range f of 10^{-4} to 10^{-1} Hz and an amplitude U , resulting in loading displacement of the form $\delta_L = \delta_{L0} + V_L t + U \sin ft$, where δ_{L0} is the displacement at $t = 0$. Amplitudes of the oscillating component result in 0.042 to 0.7 and 0.025 to 0.41 MPa changes in shear and normal traction, respectively, resolved on the fault surface. Pressure, axial load, and displacement were recorded at a rate of one sample per second in the $V_L = 0.1 \mu\text{m s}^{-1}$ experiments and averaged to as much as 5 s intervals in the $V_L = 0.001 \mu\text{m s}^{-1}$ experiments. At each combination of loading rate, frequency and amplitude, approximately 20 failure events were recorded (Table 1); this is a sufficient statistical sampling to identify strong correlation between the periodic stress and failure time. Further details of the experimental procedures and fault surface preparation are given by *Lockner and Beeler* [1999].

3. Event Catalogs From the Experiments

[10] A typical event population consists of ~ 20 failure events recorded within < 13 mm total axial displacement (Figure 3). There are event to event variations in the stress drop and in the peak failure stress which result from displacement or time-dependent changes in frictional strength. While these variations clearly influence the time of failure, such variations produce no correlation between the failure time and the phase of the oscillating stress (see Figure 4 and discussion below). For each amplitude, frequency and loading velocity combination we record the angular phase $\theta = 2\pi ft$ of the oscillating stress at the occurrence time of each failure event. Since a sine function is used, a failure event occurring at the peak in the cyclic loading displacement or stress occurs at $\theta = \pi/2$.

[11] The resulting sequence of failure events can be treated as a random walk in which each event results in a unit length step in the direction defined by its phase angle (Figure 4). If the sequence is random, the procession will

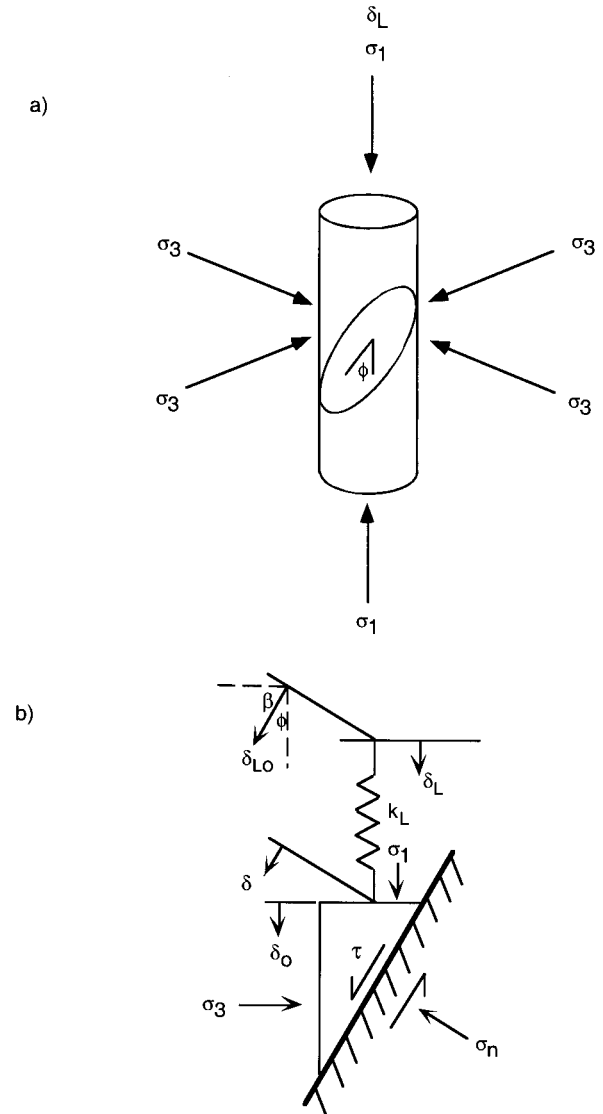


Figure 2. Experimental geometry. (a) Sample containing a fault inclined to the loading axis σ_1 , loaded under triaxial conditions, $\sigma_1 > \sigma_2 = \sigma_3$ equal to confining pressure. (b) An inclined spring and slider block representation of Figure 2a [after *Linker and Dieterich*, 1992; *He and Ma*, 1997]. The stiffness k used in analysis in this paper is the effective stiffness in the fault-parallel direction, given by $k = k_L \sin^2 \beta \cos \beta$ [Walsh, 1971; *He and Ma*, 1997], where k_L is the stiffness in the axial direction and β is the complement of the angle ϕ between the sample axis (σ_1 direction) and the fault plane; δ_L is the load point displacement in the axial direction and δ_{L0} is the load point displacement associated with k ; σ_3 is constant, consistent with the experimental geometry.

wander an average distance $D = \sqrt{N}$ from the origin, where N is the number of events. *Schuster* [1897] and *Rydelek and Hass* [1994] developed a simple expression for the probability P_{rw} that a random walk will end within a given distance D from the origin;

$$P_{rw} = \exp(-D^2/N). \quad (1)$$

Table 1. Summary of Experimental Event Catalogs of *Lockner and Beeler* [1999]^a

Exp	LB99	N	f , Hz	V_{L_2} $\mu\text{m s}^{-1}$	$\Delta\tau_{00}$ MPa	P_{rw}	$1 - P_{rw}$	P_m/P_0
5a	a10	15	0.01	0.1	0.183	0.0214	0.979	0.94
6a	a12	10	0.01	0.1	0.359	0.0026	0.997	1.43
8a		18	0.01	0.1	0.042	0.2599	0.740	
8b	a09	18	0.01	0.1	0.092	0.389	0.611	0.42
9a	a08	16	0.05	0.1	0.381	0.004	0.996	1.09
11a	a07	23	0.05	0.1	0.170	0.463	0.537	0.34
11b	a04	22	0.05	0.1	0.099	0.640	0.360	0.27
12a		18	0.05	0.1	0.056	0.413	0.587	
13a	a14	25	0.002	0.1	0.342	0.003	0.997	0.89
14a	a15	17	0.002	0.1	0.711	1. e-5	1.000	1.51
15a	a11	20	0.01	0.1	0.359	0.004	0.996	0.98
16a	a03	35	0.1	0.1	0.651	7. e-6	1.000	1.08
17a	a02	27	0.1	0.1	0.265	0.006	0.994	0.81
17b	a01	15	0.1	0.1	0.153	0.311	0.689	0.52
19a_d	b11	13	0.0004	0.01	0.688	0.001	0.999	1.17
19b_c	b10	12	0.0004	0.01	0.362	0.001	0.999	1.51
20a	b09	19	0.0004	0.01	0.127	0.0001	1.000	1.17
20b_c	b08	30	0.0004	0.01	0.094	0.038	0.962	0.58
21a_b	b12	20	0.0001	0.01	0.171	0.007	0.993	0.96
22_27	c01	20	0.02	0.0001	0.083	0.660	0.340	0.27
24a	a06	23	0.05	0.1	0.206	0.473	0.527	0.33
25	a05	24	0.05	0.1	0.104	0.507	0.493	0.33
26a	a13	23	0.002	0.1	0.171	0.863	0.137	0.22
28a_b	b04	24	0.004	0.01	0.0888	0.333	0.666	0.41
30	b01	20	0.04	0.01	0.213	0.611	0.389	0.29
31	b05	19	0.004	0.01	0.168	0.194	0.807	0.55
32	b02	27	0.04	0.01	0.265	0.030	0.970	0.69
33	b06	26	0.004	0.01	0.198	0.370	0.630	0.35
34	b07	28	0.004	0.01	0.638	6. e-6	1.000	1.21
35	b03	22	0.04	0.01	0.668	0.002	0.998	1.01

^aExp, experiment; LB99, *Lockner and Beeler* [1999].

A population containing a nonrandom component, i.e., one that is correlated with the phase of the periodic stress, will tend to produce a value of D larger than \sqrt{N} . We have determined P_{rw} for all populations (Table 1). An experiment with zero amplitude produced a population that is not correlated (Figure 4, labeled 0 MPa), whereas nonzero populations show systematic variations in the

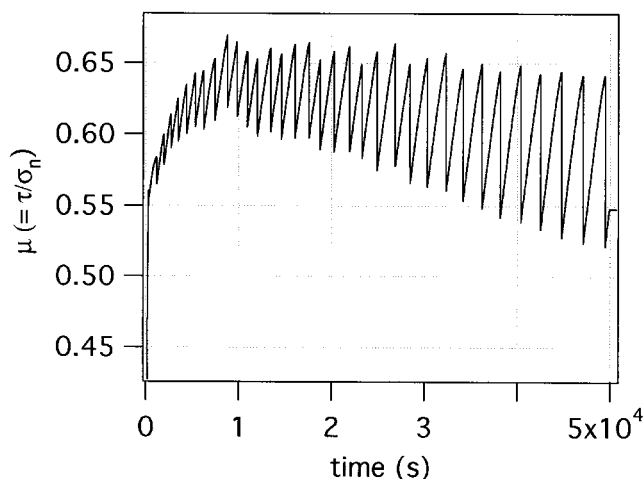


Figure 3. Friction μ , the ratio of shear stress τ to normal stress σ_n on a fault, versus time for the entire sequence of stick-slip events at 50 MPa confining pressure and $0.1 \mu\text{m s}^{-1}$ loading velocity in the experiment shown in Figure 1.

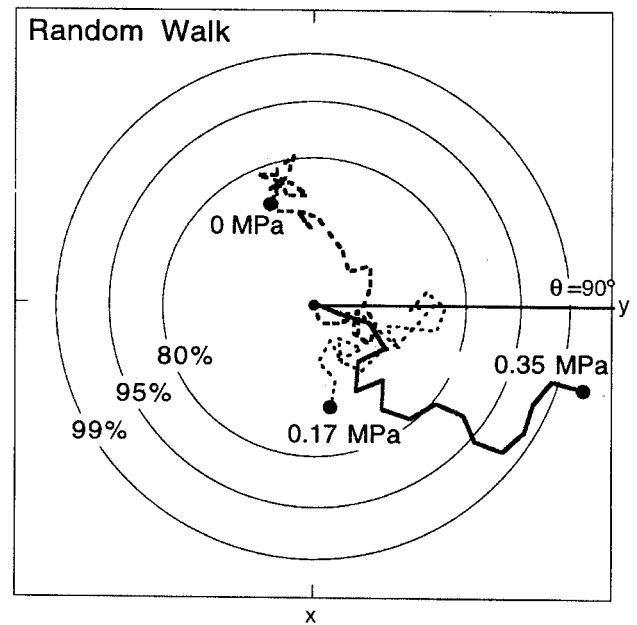


Figure 4. Examples of random walks of failure phase from three experiments from *Lockner and Beeler* [1999]. Displacement oscillation amplitudes U were 0, 2.8, and $5.5 \mu\text{m}$ (0, 0.17, and 0.35 MPa shear stress). Frequency of oscillation f was 0.05 Hz. The largest amplitude sequence showed a strong bias for events to occur with a phase of 70° (20° before peak stress). The possibility that this sequence of events could occur by random chance can be rejected at the 99% confidence level using equation (1). Both the zero amplitude and $2.8 \mu\text{m}$ sequences remained well within the limits expected for a random process. Presumably, a longer sequence of $2.8 \mu\text{m}$ amplitude events would begin to show a nonrandom drift similar to the $5.5 \mu\text{m}$ sequence.

degree of correlation with amplitude and frequency. The quantity $1 - P_{rw}$ (Table 1) expresses the probability that a sequence of failure events does not occur at random phases. At all frequencies the largest amplitude populations show strong correlation between failure time and the phase of the periodic stress, and in all cases we were able to reduce the amplitude until the occurrence of failure could no longer be distinguished from random. Figure 5 shows the $(1 - P_{rw}) = 99.5\%$ confidence level bounding populations with strong correlation between failure time and the periodic stress. In general, for each frequency the larger-amplitude stresses are better correlated than smaller-amplitude stresses.

[12] For comparison with subsequent model calculations, each population can be displayed as a probability distribution, for example, as shown in Figure 6. In Figure 6 the left-hand axis is angular probability density (rad^{-1}). The right-hand axis is the periodic component of stress which is shown for direct comparison with the probability density. The correlated populations have an approximately sinusoidal distribution with the same period as the driving stress; the amplitude of the distribution reflects the degree of correlation. On the basis of the form of the distribution and the lack of correlation in the zero amplitude population (Figure 4), we assume that the imposed stressing results in a purely random component P_0 , due to the

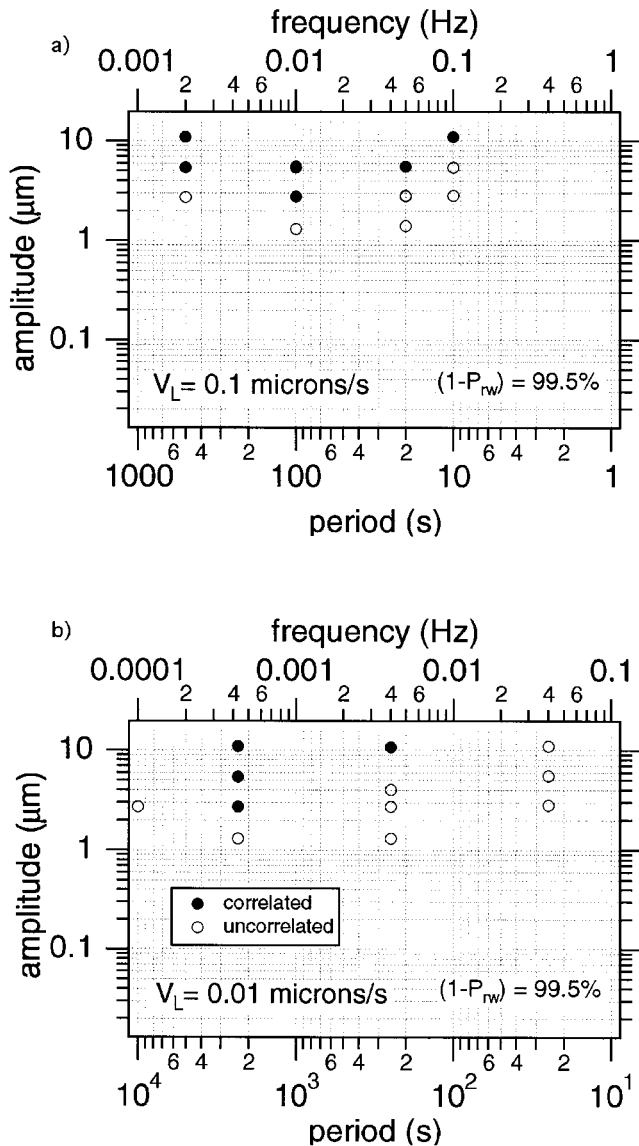


Figure 5. Summary plot of all event populations. (a) Each symbol represents a population of ~ 20 failure events which were loaded at a constant rate $V_L = 0.1 \mu\text{m s}^{-1}$ and which experienced an oscillating stress of amplitude and period indicated by the figure axes. Solid symbols are populations whose Schuster probability $(1 - P_{rw}) > 99.5\%$, equation (1), indicating a high degree of correlation between the phase at failure and the phase of the oscillating component of the loading stress. Open symbols are populations whose Schuster probability $(1 - P_{rw}) < 99.5\%$. (b) Same as Figure 5a except for $V_L = 0.01 \mu\text{m s}^{-1}$.

steady loading ($\dot{\tau} \propto V_L$), and a periodic component P_p with the same frequency as that of the periodic stress. Were the probability density (PDF) a perfect sine wave,

$$P(\theta) = P_0 + P_p = P_0 + P_m \sin(\theta - \phi_s), \quad (2)$$

is the appropriate representation [Lockner and Beeler, 1999]. Here P_0 is the average value of the PDF and represents the uniform probability, a strictly Poissonian

occurrence of events. Parameters P_m and ϕ_s are the amplitude and phase shift, respectively, of the periodic component of the PDF. As the distributions are approximately sinusoidal (Figure 6), we use equation (2) to empirically quantify the degree of correlation. Because of the small event numbers, the probability distributions (e.g., Figure 6) were smoothed using a procedure described by Lockner and Beeler [1999]. These smoothed PDFs were then fit with the sinusoid (equation (2)) to determine the amplitude P_m . The ratio P_m/P_0 , the amplitude of the distribution normalized by the average or random component, is a useful measure. Values greater

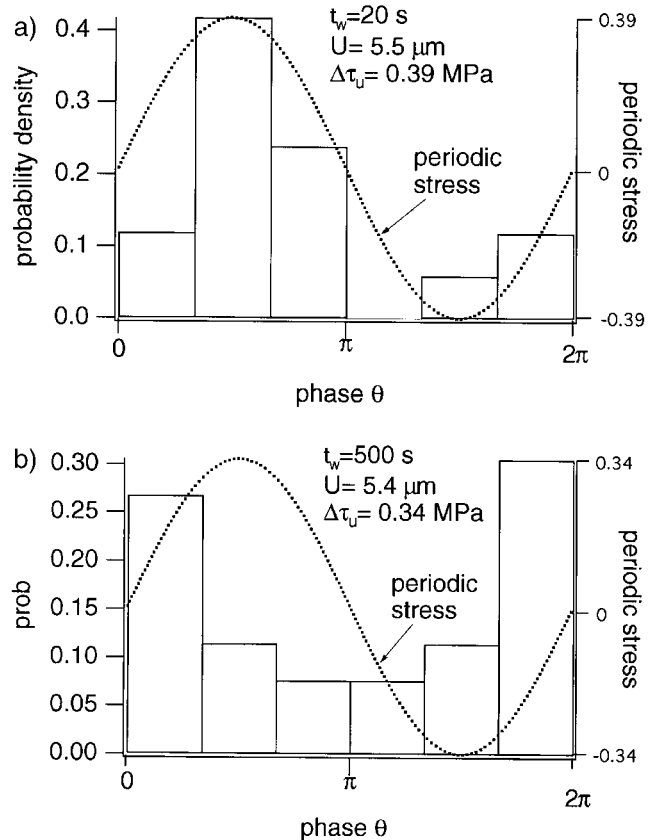


Figure 6. Example probability density distributions. (a) A histogram of the distribution of events with respect to the phase of the oscillating stress component. This population experienced a loading velocity $V_L = 0.1 \mu\text{m s}^{-1}$ and an oscillating stress of amplitude and period $U = 5.5 \mu\text{m}$ and $t_w = 20 \text{ s}$, respectively (dotted). This example is typical of the response of experimental faults to short-period stressing. The histogram is expressed as a probability density, and this example is statistically correlated with the driving stress using either equation (1) or equation (2). Note that the highest angular seismicity rate coincides with the highest stress. (b) Same as Figure 6a except for loading velocity $V_L = 0.1 \mu\text{m s}^{-1}$ and stress amplitude and period $U = 5.4 \mu\text{m}$ and $t_w = 500 \text{ s}$, respectively. This example is typical of the response of experimental faults to long-period stressing. Note that the highest angular seismicity rate coincides with the highest angular stressing rate, in contrast to the case shown in Figure 6a.

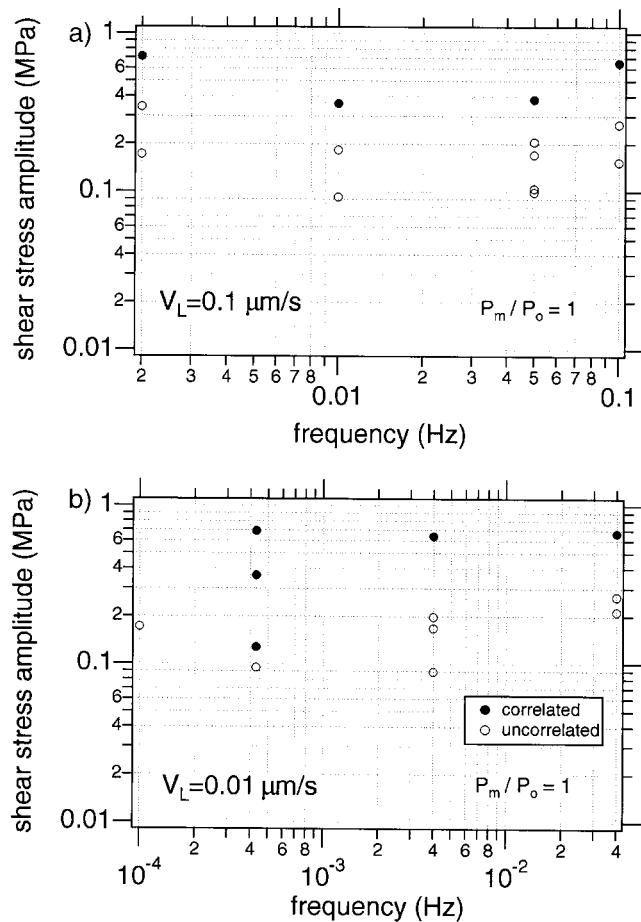


Figure 7. Summary plot of all event populations. (a) Each symbol represents a population of ~ 20 failure events which were loaded at a constant rate $V_L = 0.1 \mu\text{m s}^{-1}$ and which experienced an oscillating stress of amplitude and period indicated by the figure axes. Solid symbols are populations with ratio $P_m/P_o > 1.0$ (equation (2)), indicating a high degree of correlation between the phase at failure and the phase of the oscillating component of the loading stress. Open symbols are populations whose ratio $P_m/P_o < 1.0$. (b) Same as Figure 7a except for $V_L = 0.01 \mu\text{m s}^{-1}$.

than one indicate that the correlated response dominates failure. Small, nonzero values of P_m/P_o indicate conditions under which only a weak correlation exists between the periodic stress and failure. The shape of the contour of P_m/P_o bounding correlated and uncorrelated populations (Figure 7) is similar to the analogous Schuster probability contour (Figure 5).

4. Rate and Probability of Earthquake Occurrence

[13] In the subsequent section 5 of this paper, we use specific models of failure to simulate the laboratory populations and generate synthetic probability densities analogous to the histograms shown in Figure 6. Then, we relate those probability densities to the overall probability that a population of simulated event failure times is influenced by the periodic stress. To define the probability we first develop a

general description of earthquake rate and apply it to the case of interest, populations whose failure times have both a purely random component and a periodic component.

[14] Consider a set of seismic source faults that is subject to a constant background stressing rate, resulting in a constant failure rate r_o (seismicity rate). The population of earthquakes occurring on the faults is numbered $n = 1$ to N_T , and ordered by increasing time of failure. The reciprocal of the background seismicity rate is $1/r_o = \Delta t_b/\Delta n$, where t_b is the failure time of an event due to the background load alone. The addition of a small oscillating stress can cause the failure time of each event to be increased or decreased by an amount $t_c = t_b - t$ where t_c is the clock advance (positive values indicate that failure time is advanced, and t is time of failure). The reciprocal rate as a function of time is

$$\frac{1}{r}(t) = \frac{1}{r_o} - \frac{\Delta t_c}{\Delta n}(t). \quad (3)$$

Equation (3) can be rearranged and expressed as the seismicity rate

$$r(t) = \frac{r_o}{1 - r_o \frac{\Delta t_c}{\Delta n}(t)} = \frac{r_o}{1 - \frac{\Delta t_c}{\Delta t_b}(t)}. \quad (4)$$

This approach was developed specifically for analysis of these laboratory data sets, but it is a general formulation and can be used to model any induced change in seismicity rate, for example aftershocks [e.g., *Gomberg et al.*, 2000]. Noting that $t = \theta t_w/2\pi$, where t_w is the period of the oscillating stress, we rewrite equation (4) in a differential form as an angular seismicity rate

$$r(\theta) = \frac{r_{\theta 0}}{1 - \frac{d\phi_c}{d\theta_b}(\theta)}. \quad (5)$$

Here θ_b is the phase at failure of an event due to the background load, ϕ_c is the shift of the phase at failure induced by the oscillating stress (positive values indicate that failure is advanced), and θ is phase at failure.

[15] For a small number of events N_T occurring on a single fault, such as in our experimental study, the average angular seismicity rate is much less than one event per period ($1/2\pi$). To apply lab results to the Earth we are interested in earthquake populations consisting of the failure of multiple faults and multiple segments of individual faults. In this case, we assume that each individual fault in some large fault population would respond in the same manner as the individual faults we observed experimentally. In other words, we assume that the onset of stress drop, regardless of event size, ambient stress, and other external conditions, is controlled by a process or processes common to all faults. The angular seismicity rate in the absence of the oscillating stress is $r_{\theta 0} = N_T/2\pi$. For comparison with our experimental results we normalize equation (5) to express it as a probability density instead of an angular seismicity rate

$$P(\theta) = \frac{1}{2\pi \left(1 - \frac{d\phi_c}{d\theta_b}(\theta)\right)}. \quad (6a)$$

Alternatively, the probability density can be expressed without consideration of the phase shift simply as

$$P(\theta) = \frac{1}{N_T} \frac{dn}{d\theta}(\theta). \quad (6b)$$

For consistency with *Lockner and Beeler* [1999] and equation (2), equation (6a) can be divided into two components

$$P(\theta) = P_o + P_p(\theta) = \frac{1}{2\pi} + \frac{\frac{d\phi_c}{d\theta_b}(\theta)}{2\pi \left(1 - \frac{d\phi_c}{d\theta_b}(\theta)\right)}. \quad (7)$$

The first term on the right-hand side of equation (7), P_o represents the uniform probability due to the steady background loading, and the second term P_p is the component resulting from the periodic loading signal. Note that when the angular seismicity rate is constant, i.e., no periodic component, $dn/d\theta = r_{\theta 0} = N_T/2\pi$, and $d\phi_c/d\theta_b = 0$ so that equation (6a) or (7) define the average probability density $\bar{P}(\theta) = P_o = 1/2\pi$.

[16] Finally, we must define the degree that a synthetic population of events, with probability density calculated from equation (7), is correlated with a periodic stress of arbitrary amplitude and frequency. We use equation (1)

$$P_{rw} = \exp(-v^2 N), \quad (8)$$

with the definition $v = D/N$; v is the walkout velocity, that is, the per event walkout. As follows from *Schuster* [1897] and *Rydelek and Hass* [1994], walkout rate is defined as

$$v = \sqrt{v_{xx}^2 + v_{yy}^2}, \quad (9a)$$

where v_{xx} is the walkout velocity in the x direction ($\theta = 0$)

$$v_{xx} = \int_0^{2\pi} P(\theta) \cos\theta d\theta, \quad (9b)$$

and v_{yy} is the walkout velocity in the y direction ($\theta = \pi/2$)

$$v_{yy} = \int_0^{2\pi} P(\theta) \sin\theta d\theta, \quad (9c)$$

in the phase plot (Figure 4). Substituting equations (9) into equation (8), we find

$$P_{rw} = \exp \left\{ -N \left[\left(\int_0^{2\pi} P(\theta) \cos\theta d\theta \right)^2 + \left(\int_0^{2\pi} P(\theta) \sin\theta d\theta \right)^2 \right] \right\}. \quad (10)$$

In section 5 we evaluate specific models of failure with equations (10) and (7).

5. Analysis

[17] The summary plots of laboratory event populations (Figures 5 and 7) suggest that there are two modes of

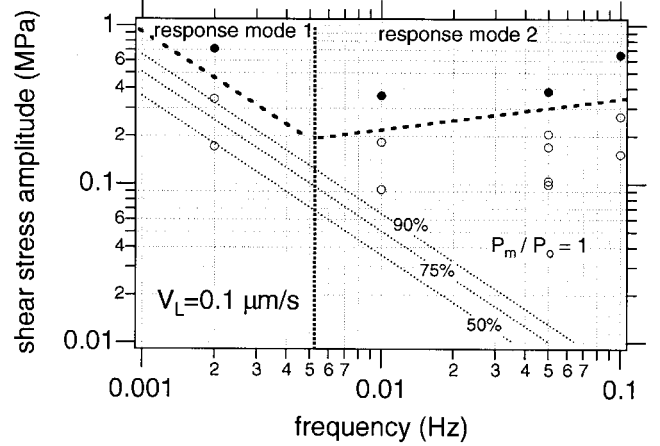


Figure 8. Summary plot of the boundaries between correlated and uncorrelated populations evaluated using the ratio $P_m/P_o > 1.0$ (equation (2)) for populations loaded at $V_L = 0.1 \mu\text{m s}^{-1}$. Same as Figure 7a except with an inferred division between the response at low frequency and at high frequency. Also shown are contours (dotted) of $(1 - P_{rw}) = 0.90, 0.75,$ and 0.50 from the threshold failure model equation (12).

response of earthquakes to periodic stress (Figure 8): a response to low-frequency stresses where the boundary separating correlated and uncorrelated populations has negative slope, and the high-frequency response where the boundary separating correlated and uncorrelated populations has positive slope. The boundary between the two response modes is marked by a characteristic time t_n . A similar division of response is suggested by the individual probability distributions of the correlated populations; the phase corresponding to the maximum event rate occurs at the peak loading velocity $\theta \approx 0$ in the low-frequency mode (Figure 6b) and at the peak stress $\theta \approx \pi/2$ in the high-frequency mode (Figure 6a). As we show in the following section, two response modes distinguished by a characteristic time are expected if failure is preceded by gradually accelerating slip of the type widely observed in previous rock fracture and rock friction experiments.

5.1. Threshold Failure Response at Low Frequency

[18] Coincidence of the maximum event rate and the peak loading velocity, seen in the experimental event populations at low frequency (Figure 6b), reflects a threshold failure response. To illustrate this coincidence, consider a population of faults at constant normal stress obeying the Coulomb failure criterion, subject to periodic loading superimposed on a constant background stressing rate. We require constant seismicity rate in the absence of the periodic component, and restrict the frequency f , amplitude $\Delta\tau_u$, and background loading rate $kV_L = \dot{\tau}$ combinations to $f\Delta\tau_u/\dot{\tau} \leq 1$ (no stress reversal). Under these constraints the seismicity rate and the probability density are proportional to the loading rate [*Lockner and Beeler*, 1999], and $P(\theta)$ (equation (7)) has an analytical solution

$$P(\theta) = \frac{1}{2\pi} + \frac{\Delta\tau_u}{\dot{\tau} t_w} \cos\theta \quad (11)$$

where $t_w = f^{-1}$ is the period of the oscillating stress. To compare simulated probabilities with our experiments, we calculate the maximum value of the ratio P_p/P_0 , which is analogous to the ratio P_m/P_0 from our data analysis with equation (2). Equation (11) has a maximum value at $\theta = 0$; thus the maximum ratio of P_p/P_0 , $(P_p/P_0)_{\max} = 2\pi\Delta\tau_u/\dot{\tau}t_w$, and the amplitude of the probability density function is directly proportional to amplitude of the periodic stress. Using equation (11), equation (10) can be evaluated directly, and we have

$$P_{rw} = \exp\left[-N\left(\frac{\Delta\tau\pi}{\dot{\tau}t_w}\right)^2\right]. \quad (12)$$

Contours of constant $1 - P_{rw}$ calculated using equation (12) with $N = 25$ and $P_{rw} = 0.1, 0.15$ and 0.5 (dotted lines, Figure 8) have a slope consistent with the boundary between correlated and uncorrelated populations in the laboratory data of *Lockner and Beeler* [1999] (heavy dashed line, Figure 8) for low-frequency stress oscillations. However, for high-frequency stress oscillations, the boundary between correlated and uncorrelated population is much higher than predicted by the contours of equation (12). For example, to induce a correlation with the driving stress at the highest frequencies in the experiments, the shear stress amplitude had to be nearly 100 times larger than would be required to induce a correlation for a fault obeying a Coulomb failure model (equation (12)). This indicates that laboratory fault failure is severely damped to high-frequency stress change, and suggests that faults have a fundamental rheological component that is lacking in threshold failure models.

5.2. Nucleation-Dominated Response at High Frequency

[19] Deviation of the observations from the Coulomb model at higher frequencies (Figure 8) results from the same rheological property that is responsible for gradual or delayed failure (Figure 1), time-dependent failure [*Griggs*, 1936; *Das and Scholz*, 1981], or static fatigue [*Scholz*, 1972; *Kranz*, 1980; *Lockner*, 1998] observed in many previous studies of rock friction and rock failure. We now illustrate specifically how delayed failure affects correlation between earthquake occurrence and periodic stressing using a simple failure model. To infer the characteristics of a model for gradual failure we use the observed acceleration to failure from our experiment with zero amplitude stress oscillation (Figure 1b). Prior to the peak strength, the sliding velocity increases, and yet the stress on the fault also increases (Figure 1a). This requires that fault strength depends positively on sliding velocity. The peak stress is reached when the sliding velocity equals the loading velocity $V = V_L$, and postpeak accelerating slip leading to unstable stress drop is accompanied by weakening. The weakening can be represented by slip weakening [e.g., *Okubo and Dieterich*, 1986; *Ohnaka et al.*, 1986; *Ohnaka and Kuwahara*, 1990]; time-dependent weakening is not appropriate because the duration of the post peak delay decreases with increasing loading velocity. Thus we infer that shear strength $\tau = g(V, \delta)$ increases with increasing velocity and decreases with displacement.

5.3. Slip- and Slip Rate-Dependent Failure Equation

[20] To model the onset of rapid slip at room temperature we assume that all inelastic deformation during faulting and

the onset of rapid slip requires cooperative slip and fracture within a localized zone. Slip may occur between asperities on opposite sides of a fault, between particles in a fault gouge, or on fracture surfaces. Regions which are fractured by crack growth during deformation may be regions of intact rock in front of a propagating rupture [*Lockner et al.*, 1991], interlocking asperities on preexisting fault surfaces [*Dieterich and Kilgore*, 1994], or particles which form grain bridges in gouge layers [e.g., *Sammis and Steacy*, 1994]. Following an approach similar to those of *Mogi* [1974] and *Savage et al.* [1996], we describe the net shear resistance at constant deformation rate by

$$\tau_* = \tau_f \frac{A_f}{A} + \tau_i \frac{A_i}{A}, \quad (13)$$

where τ_f is the shear resistance to slip, τ_i is the shear resistance necessary to break unfractured material, A is the initial unfractured area per unit mass across the incipient deforming zone, and A_f and A_i are the area per unit mass of the slipping (fractured) region and the cross-sectional area per unit mass of the unfractured portions of the fault zone, respectively. Taking $A = A_f + A_i$, we assume that $\tau_f < \tau_i$, and that A is constant. During failure, weakening with progressive slip δ results from the increase of A_f at the expense of A_i . For example, for the propagation of a single circular crack, the fractured area $A_f \propto \delta^2$. So, the fault zones of interest are unable to sustain large shear strain without loss of strength. Here for simplicity we assume that fractured area increases linearly with slip $A_f \propto C\delta$, where C is a constant with dimensions of length per unit mass, and equation (13) becomes

$$\tau_* = \tau_i - \Delta\tau \frac{\delta}{d_*}, \quad (14)$$

where we have used the definitions $\Delta\tau = \tau_i - \tau_f$ and $d_* = A/C$. Equation (14) is a slip-weakening form, previously shown to be a useful general description of quasi-static and dynamic material failure [*Palmer and Rice*, 1973; *Ida*, 1972].

[21] The resistance of fracture growth in virtually all materials depends positively on the growth rate. Figure 9 shows examples of this ‘‘subcritical’’ behavior, rate data from single cracks propagating in selected quartzofeldspathic materials: fused silica glass [*Lawn*, 1993], synthetic quartz, and Westerly Granite [*Atkinson and Meredith*, 1987]. In Figure 2 the horizontal axis is crack propagation velocity and the vertical axis is the stress intensity K_I ; stress intensity is related to the remotely applied driving stress τ and to the crack length c as $K_I \propto \tau\sqrt{c}$. Thus fracture propagation rate v_f has an exponential dependence on stress τ [e.g., *Charles and Hillig*, 1962],

$$v_f \propto \exp \tau. \quad (15)$$

We reasonably assume that the fracture propagation rate is directly proportional to the slip rate of the fault V , thus the contribution of the rate dependence of fracture propagation to the shear resistance of the fault zone is $\tau = \tau_* + \zeta \ln V/V_*$, where ζ is a constant with dimensions of stress and V_* is the slip velocity when the fault

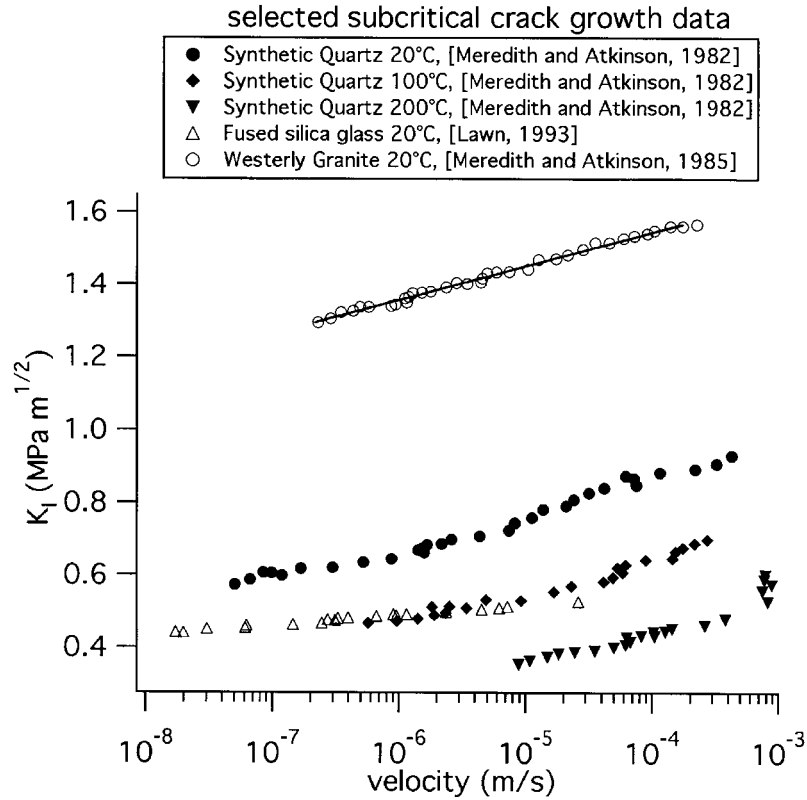


Figure 9. Subcritical crack growth in quartzofeldspathic materials. Crack stress intensity K_I versus velocity for fused silica glass [Lawn, 1993], synthetic quartz [Atkinson and Meredith, 1987], and Westerly granite [Atkinson and Meredith, 1987]. The stress intensity is proportional to the remotely applied stress; thus the vertical axis reflects the driving stress for subcritical crack extension. Also shown is a fit to the granite data using $K_I = K_0 + \zeta \ln V$, with $\zeta = 0.041 \text{ MPa m}^{1/2}$.

shear resistance is τ_* . Combining this with equation (14), we have

$$\tau = \tau_i + \zeta \ln \frac{V}{V_*} - \Delta \tau \frac{\delta}{d_*}. \quad (16a)$$

[22] Observations from deformation studies of rock friction [e.g., Dieterich, 1981; Tullis and Weeks, 1986; Blanpied *et al.*, 1998] and failure of intact rock [e.g., Scholz, 1968; Lockner, 1998], over a wide range of deformation rates, are generally consistent with equation (16a); rock shear resistance at low temperature, and low strain depends weakly on the rate of inelastic deformation. Normalizing by normal stress yields a relation for friction $\mu = \tau/\sigma_n$

$$\mu = \mu_* + a \ln \frac{V}{V_*} - \Delta \tau \frac{\delta}{d_* \sigma_n}. \quad (16b)$$

where $a = \zeta/\sigma_n$ and $\mu_* = \tau_i/\sigma_n$. Note that equation (16) is the same form as a simplification, suggested by Dieterich [1992, 1994] as appropriate for representing the onset of failure, of a particular rate and state variable constitutive equation widely used in studies of rock friction and earthquake mechanics [Ruina, 1983; Linker and Dieterich, 1992]. We have considered more complicated published

alternatives to equation (16) in detail (Appendix A) and found no superior criterion for our purposes. However, unlike more complicated rate and state formulations, equation (16) does not have a steady state value of friction and therefore cannot be used to model the effects of periodic stressing on steadily creeping faults. Some implications of periodic normal loading for earthquake occurrence on creeping faults have been investigated by Perfettini and Schmittbuhl [2001] and Perfettini *et al.* [2001].

[23] In the absence of periodic loading, equation (16a) has an analytical solution for failure time and slip velocity prior to failure, which matches the form and gross characteristics of the observed acceleration (Figure 1b) and delayed failure well (Figure 10) (equation (D1)) [Dieterich, 1992]. We calculate the failure times of fault populations with fault strengths satisfying equation (16). The faults are subjected to oscillatory loading consistent with the experimental conditions. Loading is coupled to the fault through an elastic element (spring) representing the combined elastic stiffness of the loading frame and the sample, that is $\tau = k(\delta_L - \delta)$, where k is the elastic spring stiffness and δ_L is the displacement of the load point of the spring. The analogous stiffness in the Earth is proportional to the ratio of the shear modulus and the dimension of the slipping region [Walsh, 1971]. Because there is no analytical solution for fault

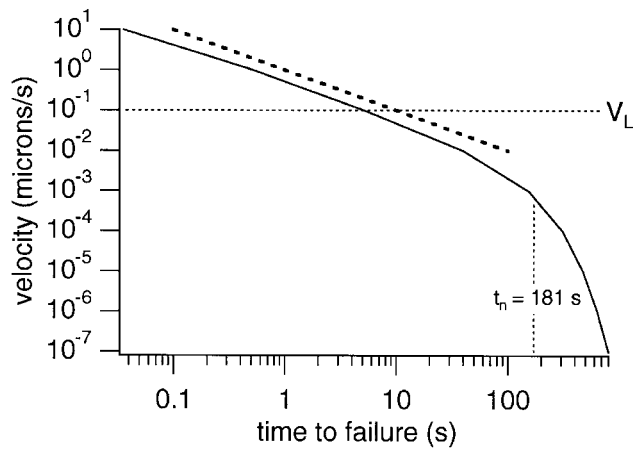


Figure 10. Accelerating failure with the simple strength equation (16). Time to failure as a function of sliding velocity was calculated using equation (A3), where the loading velocity $V_L = 0.1 \mu\text{m s}^{-1}$, the velocity at failure $V_{\text{fail}} = 30 \mu\text{m s}^{-1}$, the ratio $a\sigma_n/\dot{\tau} = 71.4\text{s}$, $\gamma/\dot{\tau} = 132.9 \text{ s } \mu\text{m}^{-1}$, and $\gamma = (\Delta\tau\sigma_n/d_* - k)$. In this example, 99% of the displacement prior to failure occurs in the 181 s prior to failure (see equations (A3)–(A5)). A line with slope -1 is shown for reference and for comparison with the acceleration to failure seen in the experiments (Figure 1b).

motion, a Runge-Kutta scheme with adaptive step size control [Press *et al.*, 1986] was used to calculate slip numerically. Care was taken to insure that errors in numerically calculated failure time do not affect the validity of our analysis. The Runge-Kutta scheme was tested against a linearly rate-dependent constitutive equation that has an analytical solution for oscillatory loading. Differences between failure time calculated by the numerical routine and the analytical solution are typically $<0.5 \text{ s}$ for calculations of 10^4 s duration. Numerical calculations with equation (16) have errors in failure time of this order. The random component in simulated populations was generated by uniformly distributing the population starting stresses over one period; this yields a uniform distribution of failure phase when $U = 0$ (a uniform background seismicity rate). The starting sliding velocity is determined from the starting stress, assuming $\delta_r = \delta_o = 0$. Because strength loss is not abrupt, we have arbitrarily defined failure as occurring when the sliding velocity reaches a threshold level $V_{\text{fail}} = 0.03 \text{ mm s}^{-1}$ or $V_{\text{fail}} = 0.1 \text{ mm s}^{-1}$. Since slip is accelerating rapidly by this time, either choice or a still higher slip rate threshold yields approximately the same failure time, and the results are not affected [e.g., Dieterich, 1992].

[24] PDFs of simulated failure events are similar to the laboratory data. At high frequency, there is essentially no phase shift between the peak seismicity rate and the peak stress amplitude (Figure 11a), as observed experimentally (Figure 6a). In a lower frequency example (Figure 11b) the duration of nucleation (150–200 s) is shorter than the period of stress oscillation (500 s), causing the peak in seismicity rate to shift toward the peak in stressing rate. For this choice of parameters the stressing rate peak and seismicity rate almost coincide. At longer periods the

stressing rate and seismicity rate peak coincide as in the data (Figure 6b) and the Coulomb model (equation (12)). The amplitude and frequency combinations defining the $(P_p/P_o)_{\text{max}} = 1.0$ boundary in the simulations are similar to the data at low frequency where the frequency dependence is negative (Figure 12), but this boundary is frequency-independent at high frequency. Thus the model reproduces a two-mode response.

[25] Although equation (16) depends on velocity and displacement, populations respond in a Coulomb-like fashion when the period of the stress perturbation t_w is longer

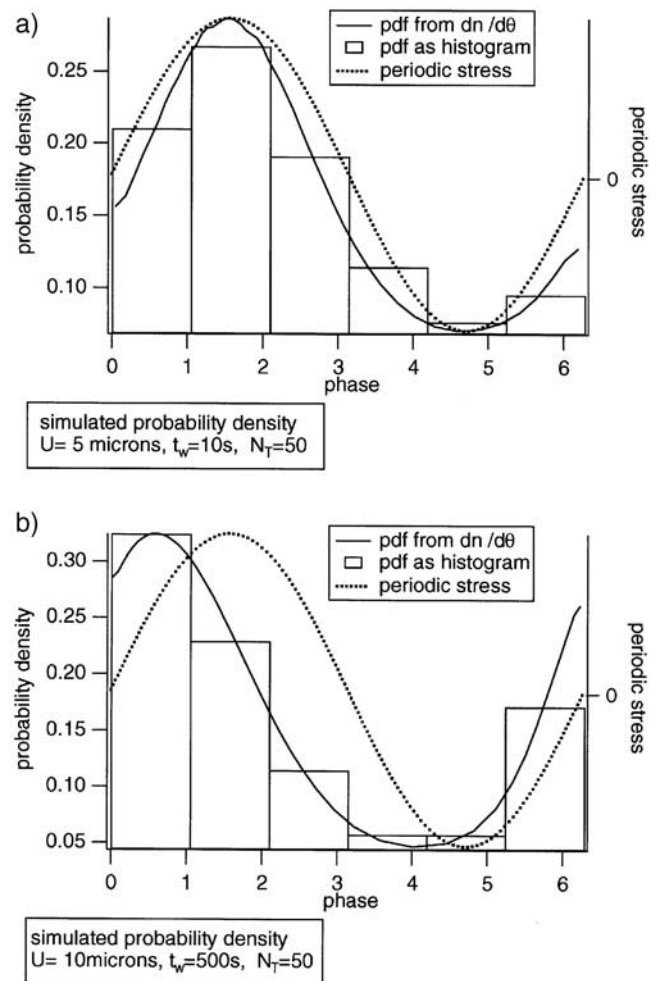


Figure 11. Simulated probability density functions for the simple rate and displacement-dependent strength equation (16) using $N_T = 50$, $V_{\text{fail}} = 30 \mu\text{m s}^{-1}$, $a = 0.005$, $\Delta\tau/d_*\sigma_n = 0.01 \mu\text{m}^{-1}$, $k/\sigma_n = 0.00071 \mu\text{m}^{-1}$. The PDF (solid line) was calculated using a centered finite difference implementation of equation (6b). The histogram is a 6 bin representation of the distribution in phase at failure of the 50 simulated failure times. The periodic component of the driving stress (dotted) is shown for comparison. (a) The results at high frequency, $U = 5 \mu\text{m}$ and $t_w = 10 \text{ s}$, are analogous to the data in Figure 6a. (b) Same as Figure 11a except for low frequency, $U = 10 \mu\text{m}$ and $t_w = 500 \text{ s}$; results are analogous to the data in Figure 6b.

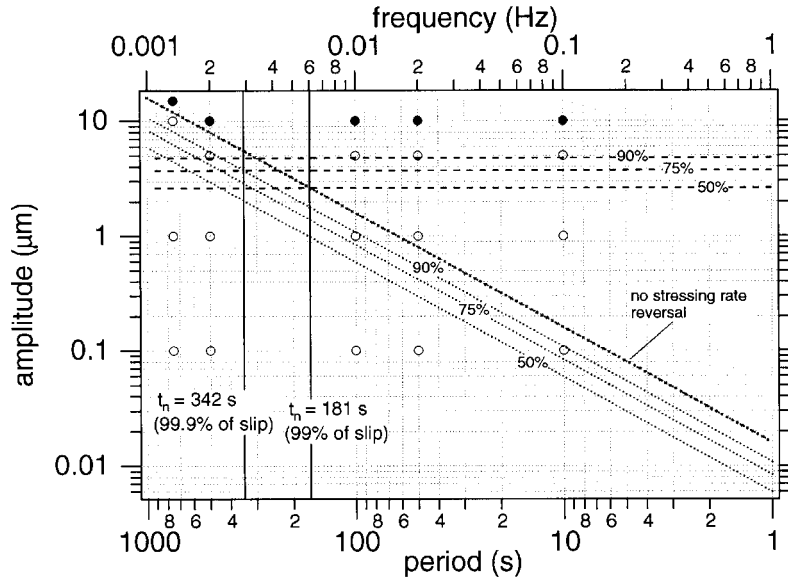


Figure 12. Model predictions. Simulated frequency dependence of triggered seismicity with a threshold failure model (dotted) and with equation (16) (symbols). Calculations with equation (16) use $a = 0.005$, $\Delta\tau/d_*\sigma_n = 0.01 \mu\text{m}^{-1}$, $N_T = 20$, $k/\sigma_n = 0.00071 \mu\text{m}^{-1}$ and $V_L = 0.1 \mu\text{m s}^{-1}$. Solid symbols are for simulated populations with $(P_m/P_0)_{\text{max}} > 1.0$, open symbols for $(P_m/P_0)_{\text{max}} < 1$. Vertical dotted lines are estimates of the duration of nucleation in the absence of the periodic stress from equations (A3)–(A5) (see Appendix D). Dotted contours of $(1 - P_{rw})$ for 0.90, 0.75, and 0.50 are predictions from the Coulomb failure model (equation (12)). Dashed contours of $(1 - P_{rw})$ are predictions of the nucleation-dominated behavior from equation (17).

than the duration of nucleation t_n . For simulations, the duration of nucleation in the absence of the periodic stress can be estimated directly (Appendix D) and we find t_n coincides with the transition between the two response modes (Figure 12). Thus $t_w \approx t_n$ defines the transition from a Coulomb-like response to a mode where the fault response is damped to high-frequency stress changes.

[26] A notable difference between predictions of equation (16) and the real populations (compare Figure 8 with Figure 12) is the lack of a frequency dependence in the boundary between correlated and uncorrelated populations of equation (16) at high frequency. The lack of frequency dependence apparently results from the logarithmic dependence of fault strength on sliding velocity in equation (16). We have conducted preliminary simulations where the slip rate dependence of the fault deviates from the logarithmic form, and the predicted boundary between correlated and uncorrelated populations is frequency-dependent. However, the quality of the experiments does not allow detailed analysis of this frequency-dependent response, so we use the simple failure law (16) to constrain the rate dependence and to extrapolate the experimental observations to natural conditions. Limitations of our analysis, arising from our use of equation (16), are discussed in section 7.

[27] Because $P(\theta)$ for equation (16) is not analytic, we obtain the probability that event populations are correlated with a periodic stress by evaluating equation (10) with equation (16) numerically. Fortunately, in the nucleation-dominated mode there are simple scaling relationships

between amplitude and walkout rate. Simulated populations with $N = 100$ (Table 2) show that the stress amplitude of the periodic component, $\Delta\tau_u$, is related to the amplitude of the probability density function as $\Delta\tau_u/a\sigma_n = 2\pi(P_p)_{\text{max}}$ (Figure 13a), equivalent to observations in rate and state simulations made by Dieterich [1987]. Furthermore, the relationship between ν and $(P_p)_{\text{max}}$ (Figure 13b) is well approximated by $\nu \approx \pi(P_p)_{\text{max}}$, the expected relationship if

Table 2. Summary of Simulated Event Catalogs Used in Figure 13^a

a	U , μm	t_w , s	P_{rw}	$(P_p)_{\text{max}}$	$(P_p/P_0)_{\text{max}}$	ν
0.005	0.1	10	0.0166	0.00226	0.0142	0.0122
0.005	1	10	0.431	0.0233	0.146	0.071
0.005	10	10	1	0.265	1.665	0.576
0.005	0.1	100	0.0134	0.00221	0.014	0.011
0.005	1	100	0.38	0.0227	0.143	0.0675
0.005	10	100	1	0.253	1.593	0.57
0.01	0.1	100	0.0097	0.00112	0.0071	0.01038
0.01	1	100	0.1156	0.0114	0.072	0.035
0.01	10	100	0.99999	0.126	0.79	0.331
0.01	0.1	10	0.0172	0.00113	0.0071	0.0105
0.01	1	10	0.172	0.0115	0.072	0.0367
0.01	10	10	0.99999	0.13	0.817	0.334
0.015	0.1	10	0.00638	0.00075	0.0047	0.01
0.015	1	10	0.0227	0.0076	0.048	0.025
0.015	10	10	0.9927	0.0826	0.519	0.23
0.015	0.1	100	0.01313	0.00075	0.00473	0.0102
0.015	1	100	0.0879	0.0076	0.048	0.0247
0.015	10	100	0.995	0.0823	0.517	0.229

^a $N = 100$, $V_L = 0.1 \mu\text{m s}^{-1}$, $\Delta\tau/\sigma_n d_* = 0.01 \mu\text{m}^{-1}$, $a = 0.005$, $k/\sigma_n = 0.0007 \mu\text{m}^{-1}$.

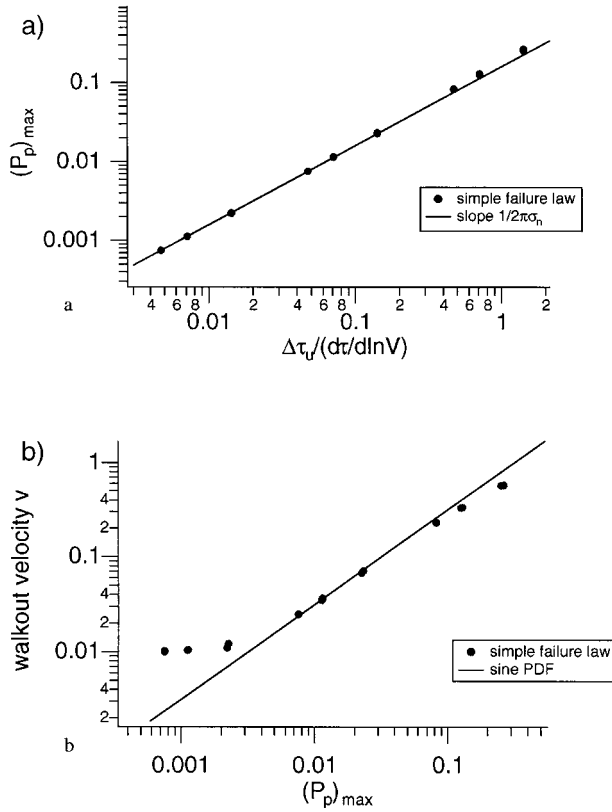


Figure 13. Scaling relationships for the simple slip and slip rate-dependent failure equation (16). (a) $(P_p)_{\max}$ versus $\Delta\tau_u/(d\tau/d\ln V)$ for simulated populations with $N = 100$. Reference line is $(P_p)_{\max} = (1/2\pi)(\Delta\tau_u/(d\tau/d\ln V))$. (b) v versus $(P_p)_{\max}$. Reference line is $v = \pi(P_p)_{\max}$, the relationship expected if $P(\theta)$ is a sine function. At low $(P_p)_{\max}$, v is independent of $(P_p)_{\max}$; this is an artifact of the numerical calculation; it is the limit of resolution of the calculation, corresponding to $1/N = 1/100$.

$P(\theta)$ were a perfect sine function (compare equation (2)). Thus the walkout velocity is $v \approx \Delta\tau_u/2a\sigma_n$, and from equation (10),

$$P_{rw} \approx \exp \left[-N \left(\frac{\Delta\tau_u}{2a\sigma_n} \right)^2 \right]. \quad (17)$$

Data from *Lockner and Beeler* [1999] (Table 1) can be used with equation (17) to directly estimate a , yielding an average value $a = 0.0045 \pm 0.0020$.

6. Discussion: Implications for Seismicity

[28] Equation (17), which expresses the probability that a population of earthquakes is not correlated with a periodic stress change, may be used to analyze observed seismicity for evidence of earthquake triggering by stress change. For example, the relation between static stress change and earthquake occurrence can be addressed with equation (17), so long as the duration of nucleation is long with respect to the period of observation but shorter than the duration of nucleation. That is, we can consider a static stress change as

a long-period stress oscillation. The particular period being unknown is not a problem, at least for faults obeying equation (16), as in the nucleation-dominated regime the degree of correlation is independent of period. We estimate the number of events necessary to detect the correlation by rearranging equation (17) to find

$$N \approx \frac{-\ln(P_{rw})}{(\Delta\tau_u/2a\sigma_n)^2}. \quad (18)$$

For illustration, *Hardebeck et al.* [1998] report that aftershocks of the Landers earthquake do not correlate with static stress changes of less 0.01 MPa [also see *Reasenber and Simpson, 1992; Simpson and Reasenber, 1994*] so we presume the period of observation (1 month) is sufficiently short for faults to be in the nucleation dominated regime and use equation (18) to estimate the number of events necessary to detect correlation. At a confidence level of 60%, using $a = 0.0045$, at depth of 5–15 km with $\sigma_n = 18 \text{ MPa km}^{-1}$, a 0.01 MPa stress change of would require $N = 6.2 \times 10^3$ to 5.5×10^4 events to detect. Thus, given the small number of available aftershocks in studies of static stress change, an apparent stress change threshold for triggering [*Hardebeck et al., 1998; Reasenber and Simpson, 1992; Simpson and Reasenber, 1994*] should arise. Another significant prediction of equation (18) is a very strong dependence of N on the stress amplitude; for example if $\Delta\tau_u$ is an order of magnitude higher, $\Delta\tau_u = 0.1 \text{ MPa}$, the number of events necessary to detect correlation at the same confidence level, $N = 60$ to 541, is 100 times smaller.

[29] While many studies find correlation between earthquakes and changes in the static Coulomb stress (see summaries by *Harris* [1998] and *Stein* [1999]), these studies also illuminate inadequacies of a Coulomb failure model. For example, Coulomb failure requires that all earthquakes occur in regions where the Coulomb stress has increased, whereas in studies of static stress change often only 60 to 70% of aftershocks meet this requirement. This may be another indication that earthquake failure is delayed as in our experiments. As evident from equation (18) and our example calculation, accounting for the amplitude of the stress change strongly influences the model-predicted degree of correlation between stress change and earthquake occurrence.

[30] Equation (18) is most appropriately used in cases of true periodic stressing. The absence of obvious triggering by the solid Earth tides, which have $f\Delta\tau_u/\dot{\tau} \gg 1$, suggests that natural faults are in the nucleation-dominated regime for the dominant tidal frequencies. In this case, the tidal period can be used as a lower bound on the duration of nucleation; i.e., typical earthquake nucleation times must exceed the daily tidal period of ~ 12.5 hours, otherwise a strong correlation would be evident. This principal conclusion of our study was inferred previously by *Knopoff* [1964], on the basis of consideration of seismological data and laboratory-observed static fatigue in rock as summarized by *Bridgeman* [1952], and by *Rydelek et al.* [1992] solely on the basis of seismological observations. We can further constrain the duration of earthquake nucleation using the results of simulations with equation (16) by noting the duration of nucleation is close to, but somewhat higher than, the frequency at the intersection of the two response

modes (Figure 12). Equating equations (12) and (17) to find the intersection is

$$t_n \approx \frac{2\pi a \sigma_n}{\dot{\tau}}. \quad (19a)$$

To evaluate equation (19a) for the San Andreas fault system, we determine the stressing rate by assuming a stress 10 MPa stress drop and 30 to 150 year recurrence, $\dot{\tau} = 0.33$ to $0.0667 \text{ MPa yr}^{-1}$, a depth range of 5–15 km with $\sigma_e = 18 \text{ MPa km}^{-1}$ (appropriate for hydrostatic fluid pressure), and our experimentally derived value of $a = 0.0045$ ($a\sigma_n = 0.4$ – 1.2 MPa). We estimate the typical duration of earthquake nucleation is 7.63–114.5 years. A less conservative estimate of the duration of nucleation is [Dieterich, 1994]

$$t_n \approx \frac{a\sigma_n}{\dot{\tau}}. \quad (19b)$$

Noting that equation (19a) somewhat overestimates the point of inflexion in Figure 12 we repeat the estimate for t_n using equation (19b) and conclude the typical duration of earthquake nucleation is 1.2 to 18.2 years.

[31] Presuming that seismic faults are in the nucleation-dominated regime with respect to the daily tidal period we can use equation (18) to estimate the number of events necessary to detect the correlation. To detect correlation at the 95% confidence level with $\Delta\tau_u = 0.001$ to 0.004 MPa , again using $a = 0.0045$, at depth of 5–15 km with $\sigma_n = 18 \text{ MPa km}^{-1}$, would require $N = 1.23 \times 10^5$ to 1.97×10^6 events. If $a = 0.01$ to 0.003 , a range expected based on other studies of rock friction, due to the strong dependence of N on a and the wide range of expected values of a , the number of events is $N = 1.36 \times 10^4$ to 8.6×10^7 . On the basis of these assumptions, confident correlation between earthquakes and the daily tides should be extremely difficult to detect, as is generally found [Vidale *et al.*, 1998].

7. Some Limitations

[32] Our laboratory-inferred value of $a\sigma_n$ (section 6) may be somewhat overestimated. By adopting equation (16) as a description of failure, we have ignored the frequency dependence of the boundary between correlated and uncorrelated populations at the highest frequencies (Figures 5 and 7). If, during the nucleation-dominated response mode, failure time is sensitive to the frequency content of the driving stress, then extrapolations of laboratory results to the Earth must consider an extrapolation in frequency which is not necessary with equation (16). On the basis of the observed frequency dependence, tidal frequencies and stressing rates would require a smaller value of $a\sigma_n$ than predicted by equation (16). We recommend additional and better constrained experiments with $N \gg 20$ to further establish and characterize this frequency dependence.

[33] Consistent with our suspected overestimate of $a\sigma_e$, previous attempts to estimate $a\sigma_n$ from observational data find much lower values than used in our extrapolations (0.4–1.2 MPa, section 6), for example, 0.035 MPa (0.35 bars) [Toda *et al.*, 1998], 0.08 to 0.09 MPa (0.8–0.9 bars) [Belardinelli *et al.*, 1999]. The Toda *et al.* [1998] and Belardinelli *et al.* [1999] data require either that the effective stress is very low (assuming $a = 0.005$ – 0.02 leads

to $\sigma_n = 1.8$ – 18 MPa), or that a is much smaller than measured in lab experiments (assuming $\sigma_n = 18 \text{ MPa km}^{-1}$ at 5–15 km yields $a = 0.00013$ – 0.001). Taking a similar approach as these previous studies we use equation (18) solved for $a\sigma_n = \Delta\tau_u/2\sqrt{-NT/\ln P_{rw}}$ with the earthquake catalog of Vidale *et al.* [1998] ($N = 13,042$) that showed no strong correlation with Earth tides and assume $P_{rw} = 0.49$ and $\Delta\tau = 0.003 \text{ MPa}$ to find $a\sigma_n = 0.20 \text{ MPa}$, which is in better agreement, but still somewhat lower than used in our extrapolation.

[34] The actual relationship between stress change and earthquake failure time is unknown. Failure time in frictional criteria, such as equation (16), is sensitive to stress changes $\Delta\mu = \Delta(\tau/\sigma_n)$, in contrast to the often used Coulomb criterion where the relevant stress change is $\Delta\sigma_c = \Delta\tau - \mu_f\Delta\sigma_n$, and μ_f is a constant coefficient of friction. As our extrapolations consider only changes in shear stress, and the shear and normal stress changes in our experiments are coupled, we can not speculate on the most appropriate stress change to use in studies of earthquakes triggered by periodic stress.

8. Summary and Conclusions

[35] Laboratory faults whose failure times correlate with an imposed periodic stress show two modes of response. Which mode is observed depends on whether the period of stress oscillation is longer or shorter than the duration of nucleation t_n . If natural faults respond in the same way as laboratory-scale faults, the absence of earthquakes triggered by the daily Earth tides requires that typical earthquake nucleation times exceed the daily tidal period. We also expect the following:

[36] 1. Seismicity should correlate strongly with the amplitude and frequency of small periodic stress of tidal magnitude if the period exceeds the duration of earthquake nucleation. This response of fault populations to stress can be represented by a strength model such as Coulomb failure where strength drop occurs when the driving stress reaches a threshold.

[37] 2. Correlation of seismicity with periodic stress should be much weaker than predicted by threshold models when the period of the driving stress is less than the duration of nucleation, in agreement with arguments made by Knopoff [1964] and Rydelek *et al.* [1992]. The weaker correlation reflects a damped response of faults to stress change. For laboratory faults the weak correlation results from a positive dependence of fault strength on deformation rate, the fault constitutive property that allows gradual failure nucleation.

[38] Our interpretation of seismic failure in laboratory rock friction experiments suggests that the duration of nucleation and the insensitivity of the onset of seismic fault slip to short-period stress changes are determined by the small dependence of subcritical crack growth rate on stress within the fault zone. If natural fault populations have the same properties as experiments, we expect a very weak correlation of earthquake occurrence with the daily tides and a minimum duration of earthquake nucleation in the shallow crust for the San Andreas system of ~ 1 year. Since our results indicate strong correlation between earthquake occurrence and periodic stresses with periods greater than the

duration of nucleation, we suggest that seasonal stress variations, for example those due to hydraulic loading from reservoirs or aquifers, or longer term climate anomalies may provide better evidence of stress triggering than the daily tides. Such long-period stress changes may also provide interpretable constraints on the duration of earthquake nucleation.

Appendix A: Friction Equations and Which Failure Law?

[39] On the basis of the observations from studies of rock friction [e.g. *Dieterich*, 1981; *Tullis and Weeks*, 1986; *Blanpied et al.*, 1998] and failure of intact rock [*Lockner*, 1998], over a wide range of deformation rates, rock shear resistance at low temperature depends weakly on the rate of inelastic deformation. This rate dependence of strength is well represented by a logarithmic dependence as in rock failure and rock friction constitutive relations [e.g., *Ruina*, 1983; *Lockner*, 1998]. A number of empirical frictional constitutive equations have been proposed, primarily to describe laboratory observations of stable sliding [e.g., *Ruina*, 1983; *Linker and Dieterich*, 1992; *Perrin et al.*, 1995]. These equations also produce stick-slip cycles, but are complicated by the inclusion of a state variable of uncertain physical origin. Here we demonstrate that none of these relationships results in a superior failure criterion for our experiments than the simple failure equation (16) used in the primary analysis in this paper. Trial calculations were performed using the rate and state friction equation

$$\frac{\tau}{\sigma_e} = \mu_* + a \ln \frac{V}{V_*} + b \ln \frac{\psi V_*}{d_c}, \quad (A1)$$

and three different forms of state variable ψ : *Ruina's* [1983] equation (14), where state depends on slip only, *Ruina's* [1983] equation (16), where state is slip- and time-dependent, and a quadratic relation of *Perrin et al.* [1995, p. 1489]. We used the procedure described in section 5.2 to generate synthetic populations of failure time, and have analyzed those populations to determine the degree of correlation with the periodic component of the loading using equations (1) and (2). With the exception of the quadratic relation of *Perrin et al.* [1995], the stress amplitude and frequency where seismicity is correlated with the driving stress of these rate and state formulations are identical, and they are identical to the results with equation (16) (Table A1). The results of the quadratic relation are offset to slightly lower amplitude, but are otherwise identical. Thus for rate and state descriptions, stress triggering by periodic loading is effectively independent of the state variable, whatever state might represent, and we can confidently use the simplified failure law equation (16). This is a result, in hindsight, that might be inferred from tidal simulations conducted by *Dieterich* [1987].

Appendix B: Sensitivity of Results to Constitutive Parameters

[40] The simple failure law (16) contains 2 free parameter combinations which affect the characteristics of

Table A1. Summary of Simulated Event Catalogs for Different Friction Constitutive Equations^a

U_i , μm	t_{ys} , s	P_{rw}	$1 - P_{rw}$	$(P_r)_{\text{max}}$	$(P_r/P_0)_{\text{max}}$	ν	State
0.1	100	0.95	0.05	0.0022	0.0136	0.052	s
1	100	0.87	0.13	0.0224	0.1407	0.0789	s
10	100	0.003	0.997	0.251	1.58	0.558	s
5	100	0.14	0.86	0.122	0.77	0.3213	s
0.1	500	0.95	0.05	0.0015	0.0092	0.048	s
1	500	0.86	0.14	0.0149	0.097	0.0285	s
5	500	0.25	0.75	0.079	0.498	0.193	s
10	500	0.016	0.984	0.165	1.035	0.398	s
15	750	0.005	0.995	0.186	1.17	0.452	s
10	750	0.06	0.94	0.122	0.765	0.302	s
1	750	0.88	0.12	0.0115	0.0724	0.023	s
0.1	750	0.95	0.05	0.0011	0.0072	0.0486	s
10	10	0.001	0.999	0.259	1.627	0.596	s
5	10	0.14	0.86	0.126	0.792	0.333	s
1	10	0.81	0.19	0.0229	0.144	0.082	s
0.1	10	0.95	0.05	0.0022	0.0139	0.053	s
10	50	0.001	0.999	0.256	1.61	0.569	s
5	50	0.24	0.76	0.125	0.78	0.326	s
1	50	0.92	0.08	0.0226	0.142	0.085	s
0.1	50	0.96	0.04	0.0022	0.138	0.053	s
10	10	0.0002	0.9998	0.306	1.92	0.66	slip
5	10	0.05	0.95	0.152	0.96	0.4	slip
1	10	0.83	0.17	0.027	0.17	0.1	slip
0.1	10	0.95	0.05	0.003	0.018	0.052	slip
10	50	0.0003	0.9997	0.313	1.97	0.63	slip
5	50	0.025	0.975	0.156	0.98	0.41	slip
1	50	0.75	0.25	0.028	0.18	0.103	slip
0.1	50	0.94	0.06	0.003	0.017	0.051	slip
10	100	0.0003	0.9997	0.31	1.95	0.63	slip
5	100	0.028	0.972	0.15	0.97	0.39	slip
1	100	0.71	0.29	0.028	0.18	0.093	slip
0.1	100	0.93	0.07	0.0027	0.017	0.049	slip
15	750	0.015	0.985	0.199	1.25	0.48	slip
10	750	0.13	0.87	0.131	0.082	0.33	slip
5	750	0.66	0.34	0.064	0.4	0.15	slip
1	750	0.99	0.01	0.012	0.078	0.029	slip
0.1	750	0.96	0.04	0.0012	0.0078	0.048	slip
10	10	0.007	0.993	0.259	1.6	0.58	slow
5	10	0.075	0.925	0.126	0.79	0.34	slow
1	10	0.92	0.08	0.023	0.14	0.084	slow
0.1	10	0.95	0.05	0.0021	0.013	0.051	slow
10	50	0.006	0.994	0.257	1.6	0.57	slow
5	50	0.068	0.932	0.126	0.79	0.34	slow
1	50	0.79	0.21	0.023	0.14	0.08	slow
0.1	50	0.94	0.06	0.0022	0.014	0.05	slow
10	100	0.001	0.999	0.25	1.58	0.56	slow
5	100	0.17	0.83	0.12	0.77	0.32	slow
1	100	0.993	0.007	0.023	0.14	0.076	slow
0.1	100	0.963	0.037	0.0021	0.013	0.05	slow
15	750	0.006	0.994	0.19	1.17	0.45	slow
10	750	0.077	0.923	0.12	0.77	0.31	slow
5	750	0.484	0.516	0.06	0.37	0.14	slow
1	750	0.928	0.072	0.012	0.07	0.024	slow
0.1	750	0.951	0.049	0.0011	0.0072	0.049	slow
5	10	0.002	0.998	0.28	1.75	0.58	quad
1	10	0.542	0.458	0.05	0.32	0.16	quad
0.1	10	0.94	0.06	0.004	0.028	0.0053	quad
5	50	0.003	0.997	0.25	1.63	0.56	quad
1	50	0.552	0.448	0.045	0.29	0.14	quad
0.1	50	0.93	0.07	0.0044	0.027	0.05	quad
5	100	0.002	0.998	0.24	1.5	0.52	quad
1	100	0.587	0.413	0.043	0.27	0.12	quad
0.1	100	0.933	0.067	0.0042	0.027	0.046	quad
15	750	0.007	0.993	0.2	1.25	0.51	quad
10	750	0.097	0.903	0.13	0.83	0.35	quad
5	750	0.634	0.366	0.065	0.41	0.15	quad
1	750	0.991	0.009	0.013	0.081	0.017	quad
0.1	750	0.958	0.042	0.0013	0.0085	0.048	quad

^a $N = 20$, $V_L = 0.1 \mu\text{m s}^{-1}$, $a = 0.005$, $b/d_c = 0.01$, $k/\sigma_e = 0.00071 \mu\text{m}^{-1}$; s, equation (16); slip, *Ruina* [1983, equation (14)]; slow, *Ruina* [1983, equation (16)]; quad, *Perrin et al.* [1995, p. 1489].

Table A2. Summary of Simulated Event Catalogs With Variable Constitutive Parameters^a

V_L $\mu\text{m s}^{-1}$	a	$\Delta\tau/\sigma_n d^*$ μm^{-1}	U, t_{vs} $\mu\text{m s}$	P_{rv}	$1 - P_{rv}$	$(P_p/P_0)_{\max}$	$(P_p/P_0)_{\max}$	ν
0.1	0.005	0.01	10 100	0.002	0.998	0.251	1.58	0.558
0.1	0.005	0.01	5 100	0.135	0.865	0.122	0.767	0.321
0.1	0.005	0.01	10 10	0.0008	0.9992	0.259	1.63	0.596
0.1	0.005	0.01	5 10	0.136	0.864	0.126	0.792	0.33
0.1	0.01	0.01	10 100	0.072	0.928	0.125	0.79	0.33
0.1	0.01	0.01	5 100	0.486	0.514	0.059	0.37	0.184
0.1	0.01	0.01	10 10	0.077	0.923	0.125	0.79	0.34
0.1	0.01	0.01	5 10	0.248	0.752	0.06	0.37	0.18
0.1	0.005	0.015	10 100	0.001	0.999	0.251	1.58	0.552
0.1	0.005	0.015	5 100	0.134	0.866	0.122	0.77	0.32
0.1	0.005	0.015	10 10	0.001	0.999	0.258	1.62	0.58
0.1	0.005	0.015	5 10	0.118	0.882	0.126	0.79	0.35
0.1	0.01	0.015	10 100	0.243	0.757	0.125	0.79	0.34
0.1	0.01	0.015	5 100	0.633	0.367	0.06	0.37	0.18
0.1	0.01	0.015	10 10	0.071	0.929	0.126	0.8	0.33
0.1	0.01	0.015	5 10	0.678	0.322	0.06	0.37	0.18
0.01	0.005	0.01	10 100	0.001	0.999	0.258	1.62	0.57
0.01	0.005	0.01	5 100	0.074	0.926	0.126	0.79	0.33
0.01	0.005	0.01	10 10	0.002	0.998	0.31	1.97	0.57
0.01	0.005	0.01	5 10	0.105	0.895	0.126	0.79	0.33
0.01	0.01	0.01	10 100	0.087	0.913	0.126	0.79	0.35
0.01	0.01	0.01	5 100	0.395	0.605	0.06	0.38	0.18
0.01	0.01	0.01	10 10	0.132	0.868	0.16	1	0.34
0.01	0.01	0.01	5 10	0.728	0.272	0.06	0.38	0.18
0.01	0.005	0.015	10 100	0.001	0.999	0.258	1.62	0.58
0.01	0.005	0.015	5 100	0.071	0.929	0.126	0.79	0.35
0.01	0.005	0.015	10 10	0.002	0.998	0.251	1.58	0.57
0.01	0.005	0.015	5 10	0.138	0.862	0.128	0.8	0.33
0.01	0.01	0.015	10 100	0.106	0.894	0.126	0.79	0.33
0.01	0.01	0.015	5 100	0.394	0.606	0.06	0.37	0.187
0.01	0.01	0.015	10 10	0.062	0.938	0.156	0.98	0.34
0.01	0.01	0.015	5 10	0.404	0.596	0.06	0.38	0.19

^a $N = 20$.

failure: a and $\Delta\tau/\sigma_n d^*$. We have conducted simulations at different values of these parameters at two different loading rates (Table A2). The correlated response of populations obeying (16) does not depend on $\Delta\tau/\sigma_n d^*$. This result confirms that of *Dieterich* [1987], who used *Ruina's* [1983] equation (16) with equation (A1), for which our equation (16) is a simplification. Thus, as suggested by the tidal simulations of *Dieterich* [1987] and the seismicity rate formulation of *Dieterich* [1994], the parameter a alone in equation (16) controls the population response to periodic stress.

Appendix C: Normal Stress Dependence

[41] Experiments by *Linker and Dieterich* [1992] show small slip-dependent changes in friction, $\mu = \tau/\sigma_n$, in response to changes in normal stress. Our experiments are conducted in a triaxial geometry (Figure 2) where the least and intermediate principal stresses are constant, and the fault is at a fixed angle ϕ to the greatest principal stress. In this configuration, fault normal stress is coupled to the shear stress and confining pressure as $\sigma_n = \sigma_3 + \tau \tan \phi$. To determine whether variations in normal stress need to be taken into account in modeling our experimental observations, we conducted calculations including the normal stress-dependent effect using constitutive equation (A1) with the state variable ψ given by

$$\frac{d\psi}{dt} = 1 - \frac{V\psi}{d_c} - \frac{\alpha\psi}{b\sigma_n} \frac{d\sigma_n}{dt}, \quad (\text{C1a})$$

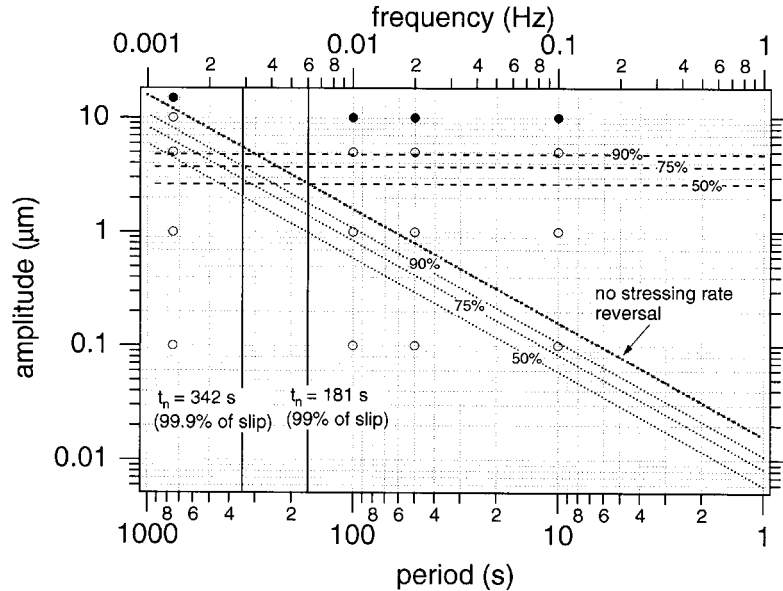


Figure A1. Variable normal stress. Model predictions for a fault at a fixed angle to the greatest principal stress at constant confining pressure (Figure 2). Simulated frequency dependence of triggered seismicity with equations (A1) and (C1). Calculations use $a = 0.005$, $b = 0.01$, $d_c = 1\mu\text{m}$, $\phi = 30^\circ$, $N_T = 20$, $\alpha = 0.23$, $\sigma_3 = 50\text{ MPa}$, $k = 0.06\text{ MPa } \mu\text{m}^{-1}$, and $V_L = 0.1\text{ } \mu\text{m s}^{-1}$. The starting value of the state variable is $\psi_0 = 10,000\text{ s}$. Solid symbols are for calculations with $(P_p/P_0)_{\max} > 1.0$; open symbols are for $(P_p/P_0)_{\max} < 1$. The probability contours shown are those corresponding to the calculation shown in Figure 12. Also shown are estimates of the duration of nucleation for the calculation shown in Figure 12.

Linker and Dieterich [1992]. Noting that in our experimental geometry $d\sigma_n = d\tau \tan\phi$, we find

$$\frac{d\psi}{dt} = 1 - \frac{V\psi}{d_c} - \frac{\alpha\psi}{b\sigma_n} \tan\phi \frac{d\tau}{dt}. \quad (C1b)$$

Failure times of fault populations were calculated numerically using oscillatory loading of the form $\delta_L = \delta_{L0} + V_L t + U \sin \omega t$ coupled through an elastic element with stiffness k , representing the stiffness of the sample and loading frame, using the procedure described in section 5.2. The results show the same response (Figure A1) as constant normal stress simulations (Figure 12). For simplicity in simulating the experiments of Lockner and Beeler [1999], elsewhere in this paper, we assume constant normal stress.

Appendix D: Characteristics of the Simple Failure Law

[42] The simple failure law equation (16) reproduces the principal aspects of failure observed in our experiments, notably, accelerating premonitory creep and delayed failure in the absence of oscillating stress (Figure 10) (see equation (D2) below), which distinguish nucleating slip from slip resulting from a threshold failure model. Equation (16) has analytical solutions for a number of simple stressing histories [Dieterich, 1994; Gomberg et al., 1998], in particular for the duration of nucleation t_n . At constant stressing rate time to failure is [Dieterich, 1992]

$$t_{yf} = -\frac{a\sigma_n}{\dot{\tau}} \ln \left[\frac{1 + \frac{\gamma}{\dot{\tau}}}{\frac{1}{V_{fail}} + \frac{\gamma}{\dot{\tau}}} \right], \quad (D1)$$

where $\gamma = (\Delta\tau/d^* - k)$. Time of failure can be found by substituting $V_{start} = V$ into (D1); V_{start} , the sliding velocity at the start of the calculation, is required to be much smaller than the loading velocity. The total accrued displacement prior to failure is

$$\delta_f = -\frac{a\sigma_n}{\dot{\tau}} \ln \left[1 - \frac{\gamma V_{start}}{\dot{\tau}} \left\{ \exp\left(\frac{\dot{\tau}}{t_{yf}}\right) - 1 \right\} \right]. \quad (D2)$$

Noting that the duration of nucleation is the time in which the majority of the precursory slip occurs, say 99% of that slip, we then solve

$$0.99\delta_f = -\frac{a\sigma_n}{\dot{\tau}} \ln \left[1 - \frac{\gamma V_n}{\dot{\tau}} \left\{ \frac{1 + \frac{\gamma}{\dot{\tau}}}{\frac{1}{V_{fail}} + \frac{\gamma}{\dot{\tau}}} - 1 \right\} \right] \quad (D3)$$

for the velocity at the onset of nucleation V_n . $V_n = V$ can then be substituted back into equation (D1) yielding t_n .

[43] **Acknowledgments.** Discussion and correspondence with T. Tullis, and J. Dieterich are gratefully acknowledged. J. Savage introduced us to Schuster's test. Numerical analyses were conducted using routines modified from a program written by J. D. Weeks. This paper was significantly improved in response to comments of T. Parsons, R. Harris, P. Rydelek, J. Vidale, and particularly Hugo Perfettini. Hugo found a significant error in our original analysis of the role of normal stress in triggering failure in the experiments.

References

Atkinson, B. K., and P. G. Meredith, Experimental fracture mechanics data for rocks and minerals, in *Fracture Mechanics of Rock*, edited by B. K. Atkinson, pp. 477–525, Academic, San Diego, Calif., 1987.

Belardinelli, M. E., M. Cocco, O. Coutant, and F. Cotton, Redistribution of dynamic stress during coseismic ruptures: Evidence for fault interaction and earthquake triggering, *J. Geophys. Res.*, *104*, 14,925–14,945, 1999.

Blanpied, M. L., C. J. Marone, D. A. Lockner, J. D. Byerlee, and D. P. King, Quantitative measure of the variation in fault rheology due to fluid-rock interactions, *J. Geophys. Res.*, *103*, 9691–9712, 1998.

Brace, W. F., and J. D. Byerlee, Stick-slip as a mechanism for earthquakes, *Science*, *153*, 990–992, 1966.

Bridgeman, P. W., *Studies in Large Plastic Flow and Fracture*, McGraw Hill, New York, 1952.

Charles, R. J., and W. B. Hillig, The kinetics of glass failure by stress corrosion, paper presented at Symposium sur la resistance due verre et les moyens de l'ameliorer, Union Sci. Cont. du Verr, Charleroi, Belgium, 1962.

Cotton, L. A., Earthquake frequency, with special reference to tidal stresses in the lithosphere, *Bull. Seismol. Soc. Am.*, *12*, 47–198, 1922.

Das, S., and C. H. Scholz, Theory of time-dependent rupture in the Earth, *J. Geophys. Res.*, *86*, 6039–6051, 1981.

Dieterich, J. H., Constitutive properties of faults with simulated gouge, in *Mechanical Behavior of Crustal Rocks: The Handin Volume*, *Geophys. Monogr. Ser.*, vol. 24, edited by N. L. Carter et al., pp. 103–120, AGU, Washington, 1981.

Dieterich, J. H., Nucleation and triggering of earthquake slip: Effect of periodic stresses, *Tectonophysics*, *144*, 127–139, 1987.

Dieterich, J. H., Earthquake nucleation on faults with rate- and state-dependent strength, in *Earthquake Source Physics and Earthquake Precursors*, edited by T. Mikumo et al., pp. 115–134, Elsevier Sci., New York, 1992.

Dieterich, J., A constitutive law for rate of earthquake production and its application to earthquake clustering, *J. Geophys. Res.*, *99*, 2601–2618, 1994.

Dieterich, J. H., and B. D. Kilgore, Direct observation of frictional contacts: New insights for state-dependent properties, *Pure Appl. Geophys.*, *143*, 283–302, 1994.

Dieterich, J. H., and B. Kilgore, Implications of fault constitutive properties for earthquake prediction, *Proc. Natl. Acad.*, 3787–3794, 1996.

Gomberg, J., N. M. Beeler, M. L. Blanpied, and P. Bodin, Earthquake triggering by transient and static deformations, *J. Geophys. Res.*, *103*, 24,411–24,426, 1998.

Gomberg, J., N. M. Beeler, and M. L. Blanpied, On rate and state and Coulomb failure models, *J. Geophys. Res.*, *105*, 7857–7872, 2000.

Griggs, D. T., Deformation of rocks under high confining pressure, *J. Geol.*, *44*, 541–577, 1936.

Hardebeck, J. L., J. J. Nazareth, and E. Hauksson, The static stress change triggering model: Constraints from two southern California aftershock sequences, *J. Geophys. Res.*, *103*, 24,427–24,437, 1998.

Harris, R. A., Introduction to special section: Stress triggers, stress shadows, and implications for seismic hazard, *J. Geophys. Res.*, *103*, 347–358, 1998.

He, C., and S. Ma, Dynamic fault motion under variable normal stress condition with rate and state friction, *Proc. Int. Geol. Congr.*, *30th*(14), 41–52, 1997.

Heaton, T. H., Tidal triggering of earthquakes, *Bull. Seismol. Soc. Am.*, *72*, 2181–2200, 1982.

Ida, Y., Cohesive force across the tip of a longitudinal shear crack and Griffith's specific surface energy, *J. Geophys. Res.*, *77*, 3796–3805, 1972.

Johnson, T., Time dependent friction of granite: Implications for precursory slip on faults, *J. Geophys. Res.*, *86*, 6017–6028, 1981.

Klein, F. W., Earthquake swarms and the semidiurnal solid Earth tide, *Geophys. J. R. Astron. Soc.*, *45*, 245–295, 1976.

Knopoff, L., Earth tides as a triggering mechanism for earthquakes, *Bull. Seismol. Soc. Am.*, *54*, 1865–1870, 1964.

Kranz, R. L., The effects of confining pressure and stress difference on static fatigue of granite, *J. Geophys. Res.*, *85*, 1854–1866, 1980.

Lawn, B., *Fracture of Brittle Solids*, 378 pp., Cambridge Univ. Press, New York, 1993.

Linker, M. F., and J. H. Dieterich, Effects of variable normal stress on rock friction: Observations and constitutive equations, *J. Geophys. Res.*, *97*, 4923–4940, 1992.

Lockner, D. A., A generalized law for brittle deformation of Westerly granite, *J. Geophys. Res.*, *103*, 5107–5123, 1998.

Lockner, D. A., and N. M. Beeler, Premonitory slip and tidal triggering of earthquakes, *J. Geophys. Res.*, *104*, 20,133–20,151, 1999.

Lockner, D. A., J. D. Byerlee, V. Kuksenko, A. Ponomarev, and A. Sidorin, Quasi-static fault growth and shear fracture, *Nature*, *350*, 39–42, 1991.

Meredith, P. G., and B. K. Atkinson, High-temperature crack propagation in quartz: Experimental results and application to time-dependent earthquake rupture, *Earthquake Predict. Res.*, *1*, 377–391, 1982.

Meredith, P. G., and B. K. Atkinson, Fracture toughness and subcritical crack growth during high-temperature tensile deformation of westerly granite and black gabbro, *Physics Earth Planet. Inter.*, *39*, 33–51, 1985.

- Mogi, K., On the pressure dependence of strength of rocks and the Coulomb fracture criterion, *Tectonophysics*, 21, 273–285, 1974.
- Ohnaka, M., and Y. Kuwahara, Characteristic features of local breakdown near a crack-tip in the transition zone from nucleation to unstable rupture during stick-slip shear failure, *Tectonophysics*, 175, 197–220, 1990.
- Ohnaka, M., Y. Kuwahara, K. Yamamoto, and T. Hirasawa, Dynamic breakdown processes and the generating mechanism for high-frequency elastic radiation during stick-slip instabilities, in *Earthquake Source Mechanics*, *Geophys. Monogr. Ser.*, vol. 37, edited by S. Das, J. Boatwright, and C. H. Scholz, pp. 13–24, AGU, Washington, D.C., 1986.
- Okubo, P. G., and J. H. Dieterich, State variable fault constitutive relations for dynamic slip, in *Earthquake Source Mechanics*, *Geophys. Monogr. Ser.*, vol. 37, edited by S. Das, J. Boatwright, and C. H. Scholz, pp. 25–35, AGU, Washington, D.C., 1986.
- Palmer, A. C., and J. R. Rice, The growth of slip surfaces in the progressive failure of over-consolidated clay, *Proc. R. Soc. London, Ser. A*, 332, 527–548, 1973.
- Perfettini, H., and J. Schmittbuhl, Periodic loading on a creeping fault: Implications for tides, *Geophys. Res. Lett.*, 28, 435–438, 2001.
- Perfettini, H., J. Schmittbuhl, J. R. Rice, and M. Cocco, Frictional response induced by time-dependent fluctuations of the normal loading, *J. Geophys. Res.*, 106, 13,455–13,472, 2001.
- Perrin, G., J. R. Rice, and G. Zheng, Self-healing slip pulse on a frictional surface, *J. Mech. Phys. Solids*, 43, 1461–1495, 1995.
- Press, W. H., B. P. Flannery, S. A. Teukolsky and W. T. Vetterling, *Numerical Recipes: The Art of Scientific Computing*, Cambridge Univ. Press, New York, 1986.
- Reasenber, P. A., and R. W. Simpson, Response of regional seismicity to the static stress change produced by the Loma Prieta earthquake, *Science*, 255, 1687–1690, 1992.
- Ruina, A. L., Slip instability and state variable friction laws, *J. Geophys. Res.*, 88, 10,359–10,370, 1983.
- Rydelek, P. A., and L. Hass, On estimating the amount of blasts in seismic catalogs with Schuster's method, *Bull., Seismol. Soc. Am.*, 84, 1256–1259, 1994.
- Rydelek, P. A., I. S. Sacks, and R. Scarpa, On tidal triggering of earthquakes at Camp Flegrei, Italy, *Geophys. J. Int.*, 109, 125–1376, 1992.
- Sammis, C. G., and S. J. Steacy, The micromechanics of friction in a granular layer, *Pure Appl. Geophys.*, 142, 777–794, 1994.
- Savage, J. C., J. D. Byerlee, and D. A. Lockner, Is internal friction, friction?, *Geophys. Res. Lett.*, 23, 487–490, 1996.
- Scholz, C. H., Mechanism of creep in brittle rock, *J. Geophys. Res.*, 73, 3295–3302, 1968.
- Scholz, C. H., Static fatigue in quartz, *J. Geophys. Res.*, 77, 2104–2114, 1972.
- Schuster, A., On lunar and solar periodicities of earthquakes, *Proc. R. Soc. London*, 61, 455–465, 1897.
- Simpson, R. W., and P. A. Reasenber, Earthquake-induced static stress changes on central California faults, in *The Loma Prieta, California Earthquake of October 17, 1989-Tectonic Processes and Models*, *U.S. Geol. Surv. Prof. Pap.*, 1550, F55–F89, 1994.
- Stein, R. S., The role of stress transfer in earthquake occurrence, *Nature*, 402, 605–609, 1999.
- Toda, S., R. S. Stein, P. A. Reasenber, J. H. Dieterich, and A. Yoshida, Stress transferred by the 1995 $M_w = 6.9$ Kobe, Japan, shock: Effect on aftershocks and future earthquake probabilities, *J. Geophys. Res.*, 103, 24,543–24,565, 1998.
- Tullis, T. E., and J. D. Weeks, Constitutive behavior and stability of frictional sliding of granite, *Pure Appl. Geophys.*, 124, 384–414, 1986.
- Vidale, J. E., D. C. Agnew, M. J. S. Johnston, and D. H. Oppenheimer, Absence of earthquake correlation with Earth tides: An indication of high preseismic fault stress rate, *J. Geophys. Res.*, 103, 24,567–24,572, 1998.
- Walsh, J. B., Stiffness in faulting and in friction experiments, *J. Geophys. Res.*, 76, 8597–8598, 1971.
- Weeks, J. D., N. M. Beeler, and T. E. Tullis, Glass is like a rock, *Eos Trans. AGU*, 72(44), 457, Fall Meet. Suppl., 1991.

N. M. Beeler and D. A. Lockner, U.S. Geological Survey, 345 Middlefield Road, MS 977, Menlo Park, CA 94025, USA. (nbeeler@usgs.gov; dlockner@usgs.gov)